ABSTRACT

Title of Document: ROLL CONTROL FOR UAVs BY USE OF A VARIABLE SPAN MORPHING WING

Janisa Jernard Henry, Master of Science, 2005

Directed By: Dr. Darryll J. Pines, Ph.D., Department of Aerospace Engineering

This thesis presents variable span wing morphing (VSWM) as an effector of roll control for unmanned aerial vehicles (UAVs). In this study, the roll coefficients obtained from VSWM are quantified by theoretical and experimental data and compared with typical aileron roll coefficients. We see that small changes in span are an effective alternative to conventional ailerons for producing roll. The standard six-degree of freedom (6-DOF) model that describes aircraft dynamics is revisited. We derive and examine the extra inertial terms that morphing introduces into the moment equations of the 6-DOF model. In this thesis, we derive simple expressions for these additional terms. In particular, we are able to extract a single degree of freedom model by considering the case of a pure roll. This model describes the dynamics of an aircraft executing a pure roll by means of span morphing. The critical distinction between the well-known aileron model and the span model derived in this thesis is clear. The span model contains an additional term whose behavior tends to modify the total damping.

ROLL CONTROL FOR UAVs BY USE OF A VARIABLE SPAN MORPHING WING

By

Janisa Jernard Henry

Thesis submitted to the Faculty of the Graduate School of the
University of Maryland, College Park, in partial fulfillment
of the requirements for the degree of
Master of Science
2005

Advisory Committee:
Professor Dr. Darryll Pines, Chair
Dr. John D. Anderson, Professor Emeritus
Dr. Alison Flatau, Professor

Dedication

This work is dedicated to the loving memory of my grandmothers, Eloisa Leontine Henry and Ilva Carmen Rudolfo.

Acknowledgements

Thanks be to Almighty God, whose presence has been the stabilizing force throughout the entire process of researching for, and writing this document.

To my parents and family members, whose love, guidance and sacrifice are inestimable, a very, very, special thank you.

I am especially thankful to my academic advisor, Dr. Darryll J. Pines, for affording me the opportunity to work on this project, and for his constant encouragement and support. I want to express enormous gratitude to Dr. Jewel B. Barlow, whose guidance saw me through chapter 5, from its beginning to end. I could not have completed this document without your assistance.

Special thanks to Dr. Paul D. Samuel, who patiently guided me through numerous iterations of this document. Thank you, Dr. Allen Winkelmann, for graciously affording me the use of your laboratory, testing equipment and expertise. To Les Yeh and the others at the Glenn L. Martin Wind Tunnel, your assistance has been greatly appreciated.

I am truly appreciative of the selfless assistance offered to me by Ashish Purekar and Adrian Hood. Thank you very much Felipe Bohorquez, for reading my papers and giving me solid advice. Credit must be given to Joseph Conroy and Celestine Wakha, who were always willing to help me with any problem. To Daniel Everson and Ron Couch, who so graciously and patiently assisted me with the formatting of this document, thank you. You've saved me several hours of frustration!

I would like to extend a very big vote of thanks to Mrs. Patricia Baker and Dr. Mary Bowden. I could not have completed this work without you. Thank you so very much.

I am grateful to Dr. Anubhav Datta who dispensed wisdom with wit and humor. You're a good friend. I would like to recognize Dr. Suneel Sheikh, and Matthew Strube who fielded my numerous questions and always made themselves available.

To Lauren Chung: it has been a pleasure knowing you. We have shared so much as we strove to complete our theses. Thanks for being my friend. Suzanne Ruddy, you are a wonderful friend. Best wishes for your new job and congratulations on your engagement. To my friend Stacey Thomas: you were always there when I needed someone to talk to. You've put up with long periods of silence as I buried myself in my ivory tower. Thanks for understanding and for simply being there.

To Dr. Melva Brown and Dr. and Mrs. Myron Ottley who so graciously opened their homes to me, even when I was miles away from my own. Thank you.

Table of Contents

Dedication ii

Acknowledgements iii

Table of Contents v

List of Tables vii

List of Figures viii

Nomenclature x

Chapter 1: Introduction 1

Chapter 2: Literature Survey 4

2.1 State of the Art in Performance Morphing 4

2.1.1 Variable Sweep Wings 5

2.1.2 Variable Cambered Wings 7

2.1.3 Variable Span Wings 10

2.2 State of the Art in Roll Control 11

2.2.1 Conventional Roll Control 12

2.2.2 Morphing Roll Control 18

Chapter 3: Theoretical Prediction of VSMW Roll Moment 24

3.1 Finite Wing Theory Prediction 24

3.2 Comparison between Theoretical VSMW and Aileron Roll Coefficients 27

Chapter 4: Maryland Variable Span Morphing Wing 31

4.1 Wind Tunnel Model Development 32

4.1.1 The Pneumatic Actuator 33

4.1.2 Ribs 35
4.1.3 The Skin 37
4.1.4 Length Sensors 37
4.2 Wing Body Integration 39
4.3 Wind Tunnel Methodology 40
4.4 Aerodynamic Results 42
Chapter 5: Dynamics 50
5.1 Derivation of Morphing Moment Equations 51
5.2 Separation of Moment Equations into Baseline and Perturbation Terms 54
5.3 Special Case of a Steady Roll 63
5.4 Aerodynamic Considerations 66
5.4.1 Ordinary Differential Equation (ODE) Describing Steady Roll by VSWM ... 66
5.4.2 Comparison between VSMW ODE and Aileron ODE 69
Chapter 6: Conclusions and Future Work 72
Bibliography 74

List of Tables

Table 1: Data Showing Trends Illustrated in Figure 17…….....29

Table 2: Matrix of Angles of Attack for Varying Airspeeds and Wingspan Configuration…….....41

Table 3: Dimensions of Fuselage and Half Wing …….....46

Table 4: Lift Discrepancy for 40%-40% Baseline Case……47

Table 5: Aircraft Dimensions…….60

Table 6: Morphing Geometry Nonlinear Dynamics Equations…….....62

Table 7: Special Case of a Steady Roll……..65

Table 8: Comparison between 1-DOF Aileron Model and 1-DOF Variable Span Model…….....69

List of Figures

Figure 1: LIG-7 Variable Chord Wing Aircraft……...4

Figure 2: Compressibility Effect for Mach <1…….....5

Figure 3: B-1BLancer……..6

Figure 4: F-14Tomcat……..7

Figure 5: Variable Camber Wing…….....9

Figure 6: NASA Dryden Inflatable Wing in Baseline and Inflated States…….....9

Figure 7: Gevers Variable Span Aircraft……...11

Figure 8: Operation of Aileron Spoiler……..14

Figure 9: Aileron Spoilers……..15

Figure 10: Jet Spoiler…….....17

Figure 11: Wide Area Surveillance Projectile (WASP)……17

Figure 12: Symmetric Morphing on 24 -in Span Vehicle…….....19

Figure 13: Kevlar Threads on Underside of 12-in MAV……...21

Figure 14: 12-in MAV in Undeflected and Asymmetrically Morphed States……...21

Figure 15: Hyper Elliptic Morphable Wing……..23

Figure 16: Theoretical Roll Moment from VSMW……...26

Figure 17: Comparison between Theoretical VSMW Roll Moment and Theoretical Aileron Roll Moment…….....28

Figure 18: Ergo-Help Pneumatic Actuators……...33

Figure 19: Ergo-Help Pneumatic Spar Functional Design……34

Figure 20: Variable Span Morphing Wing Airfoil Design……35

Figure 21: Rib Sections from Root, Middle and Tip Elements…….....36

Figure 22: Fully Extended Wing in Extended Configuration……...37

Figure 23: Potentiometer Mounted on Rack and Pinion……37

Figure 24: Integration of Rack into Middle and Tip Ribs…….....38

Figure 25: Middle Element Attachment and Sensor……..38

Figure 26: Wing Body Integration…….....39

Figure 27: Wind Tunnel Tests of Wing Body Model in Fully Retracted and Fully Extended Configurations……...41

Figure 28: Theoretical and Experimental Roll Moment Coefficient from VSMW……...44

Figure 29: Flow Visualization of Pressure Losses at Seams and Tip...…….....45

Figure 30: Comparison between Aileron and Span Roll Coefficient……48

Figure 31: Inertial and Body-Fixed Coordinate Frames……51

Figure 32: Sequence of Events during Asymmetric Morphing…….....57

Figure 33: Location of Element 1 and Element 2……..60

Nomenclature

α	Angle of attack
a_0	Infinite Wing Lift Curve Slope
AR	Aspect Ratio
c	Mean Chord
H	Angular Momentum
I_{x_0}	Symmetric Roll Inertia
I_{y_0}	Symmetric Pitch Inertia
I_{z_0}	Symmetric Yaw Inertia
M_t	Total Aircraft Mass
ω	Angular Velocity Vector
q_∞	Dynamic Pressure
r	Radial Vector from Elemental Mass to Aircraft Center of Gravity
μ	Mach Angle
v	Velocity Vector of Elemental Mass
v_c	Velocity Vector of Aircraft Center of Gravity

Chapter 1: Introduction

Most aerial vehicles are designed to function at some optimum point that satisfies a single mission objective such as long-loiter intelligence, surveillance, and reconnaissance (ISR), or attack. This point exists within a certain envelope, beyond whose bounds aircraft performance and efficiency deteriorate. To a significant extent, the level of performance attainable by such a vehicle in accomplishing its mission is a dictate of vehicle geometry.

Recent advances in materials science offer a plethora of opportunities to the aerospace community. Smart materials such as memory shape alloys and embedded actuators present the exciting possibility of designing a variable geometry aircraft [1]. This concept, known as morphing, enables the aircraft geometry to be precisely tailored to changing requirements at various phases of flight. Morphing also offers the possibility of integrating several mission capabilities into a single platform [2]. In addition to enhanced performance and efficiency, morphing can be used to improve vehicle maneuverability [2]. While the development of variable geometry air vehicles has primarily been associated with high-speed manned aircraft, this technology would serve to expand the flight envelope and improve the performance of unmanned aerial vehicles (UAVs). The ultimate goal of the Morphing UAV program, as outlined by the NASA Aircraft Morphing Program, is to build and demonstrate a seamless, aerodynamically efficient aerial vehicle capable of radical shape change [1].

The variable-span morphing wing under consideration is one whose wingspan can change in response to pilot command [3]. Wings with large spans have good range and fuel

efficiency, but lack maneuverability and have relatively low cruise speeds. To the contrary, aircraft with short, stubby wings are faster and highly maneuverable, but show poor aerodynamic efficiency [4]. A variable span wing can potentially integrate into a single aircraft the advantages of both designs, making this emerging technology especially attractive for military unmanned aerial vehicles.

Morphing technologies offer the fringe benefit of controlling aircraft dynamics.
In a conventional wing configuration, roll control is achieved by the use of ailerons that are deflected such that lift is increased on one wing and decreased on the other, thus creating a roll moment [4]. In the telescoping wing developed at the University of Maryland [26], the use of ailerons is not feasible due to the overlapping of skins and the limited internal wing space.

This thesis explores the idea of using variable span wing morphing as an effector of roll control for UAVs. Roll control can be achieved without ailerons when a span difference exists between the two half wings, with the resulting lift differential yielding a roll moment. This control scheme eliminates the need for additional actuators while minimizing drag since no large span-wise wing discontinuities are present. A reduction in weight is realized since bulky actuators for ailerons are eliminated.

In this study, the roll coefficients obtained from VSWM are quantified by theoretical predictions and wind tunnel test data. We see that small span changes are sufficient to provide roll coefficients that are equivalent to those obtained from aileron deflection. In

order to study the dynamics associated with morphing aircraft it is necessary to revisit the six-degree of freedom (6-DOF) equations that describe aircraft dynamics. Morphing introduces extra terms that describe time variant inertias. In this thesis, we derive simple expressions for these additional terms. In particular, we consider the case of a steady roll. The resulting ordinary, first-order differential equation (ODE) illustrates a critical difference between an aircraft using variable span morphing for roll control and one that uses ailerons for roll control: variable span morphing induces an additional damping term into the resulting ODE.

Chapter 2 of this document presents a survey of the state of the art in performance morphing and control morphing. In the third chapter, we examine the theory behind the use of a variable span morphing wing (VSMW) to produce a roll moment. The fourth chapter describes the development of the University of Maryland VSMW, its integration to a generic fuselage body and wind tunnel tests on this wing body model. In addition, a comparison between the theoretically predicted and experimentally determined roll coefficients is presented. In Chapter 5, the six-degree of freedom equations that describe the dynamics of a morphing aircraft are derived and discussed. Chapter 6 concludes and summarizes the work in this thesis and makes recommendations for future work.

Chapter 2: Literature Survey

2.1 State of the Art in Performance Morphing

Performance morphing is the idea of using morphing to improve aircraft efficiency, and in so doing, augmenting the flight envelope. This idea is not a new one. For example, in a 1920 NACA report, H. F Parker described a method to increase an aircraft's forward speed by using a variable camber wing [5]. The philosophy behind the Parker Variable Camber Wing was to diminish drag incurred at higher speeds by altering the wing profile. In 1932, a type of variable chord wing designed by Razdviznoe Krylo was implemented on the LIG-7, shown in figure 1. The surface of this wing was extended to increase lift during take-off and landing, and retracted during cruise. In this section, the various approaches to performance morphing are described and discussed.

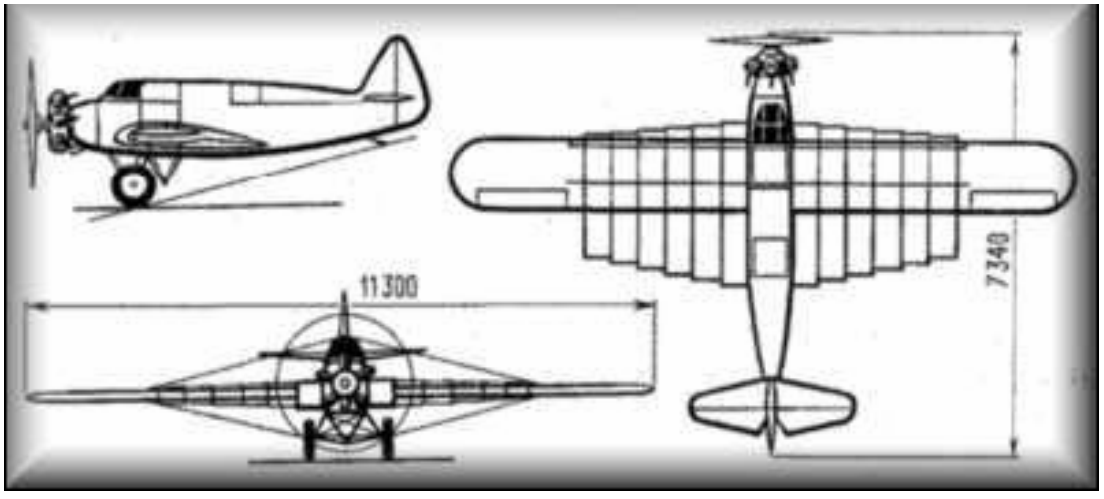

Figure 1: LIG-7 Variable Chord Wing Aircraft

2.1.1 Variable Sweep Wings

Wing sweep is used to alleviate compressibility effects. Its benefits are two-fold: in subsonic aircraft, sweep delays the onset of drag divergence by increasing the wing's critical Mach number, M_{cr}. In supersonic flight, sweep allows for the reduction of wave drag [7]. Figure 2 demonstrates the first effect. When a sweep angle, Λ is introduced, the airfoil effectively sees $M_\infty \cos\Lambda$, the component perpendicular to its leading edge. As such, the actual free-stream Mach number can be higher than M_{cr} before drag divergence phenomena are encountered. As a rule of thumb, the following relationship is true [8]:

$$M_{cr}airfoil < M_{cr}sweptwing < \frac{M_{cr}airfoil}{\cos\Lambda} \tag{2.1.1}$$

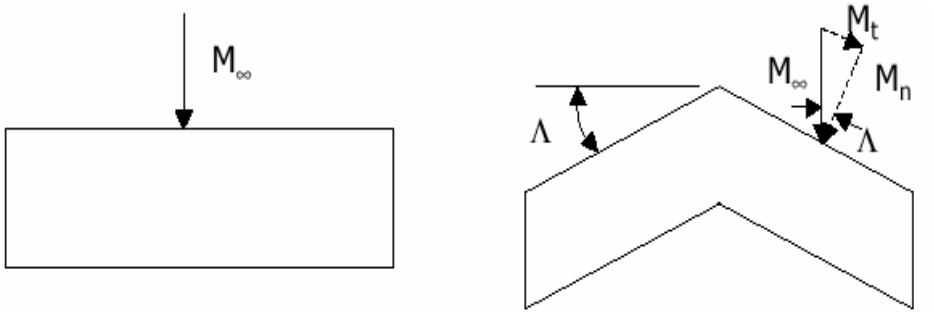

Figure 2: Compressibility Effect for Mach <1

Some supersonic flows are accompanied by oblique shocks. The pressure ratio across an oblique shock is given by [9]:

$$\frac{p_2}{p_1} = 1 + \frac{2\gamma}{\gamma+1}\left(M_{n,1}^2 - 1\right) \tag{2.1.2}$$

$$M_{n1} = M_1 \sin\beta \tag{2.1.3}$$

If the wing is swept such that its wedge angle $\theta > \mu$, the normal component to the leading edge, M_{n1}, is supersonic; hence, an oblique shock is generated with a large attendant wave drag. However, if the wedge angle $\theta < \mu$, the shock angle β is decreased such that $M_{n1} = M_1 \sin\beta < 1$ with a commensurate decrease in pressure. Sweep is not always desirable. At subsonic speeds, the $\frac{L}{D}$ ratio is decreased with an increase in sweep; however, in supersonic flight, $\frac{L}{D}$ is independent of sweep.

Examples of aircraft that use variable sweep wings include the B-1B Lancer and the F-14 Tomcat. The B-1B Lancer, shown in Figure 3, is a long-range heavy bomber in service with the United States Air Force since 1986 [10]. Its blended wing body configuration and variable sweep wing enhance range and speed and increase survivability. During takeoff, landing and high-altitude maximum cruise, the wings are kept in the forward position. Aft wing settings of 15°, 25°, 45°, 55°, and 67.5° were cleared for use at high subsonic and supersonic flights.

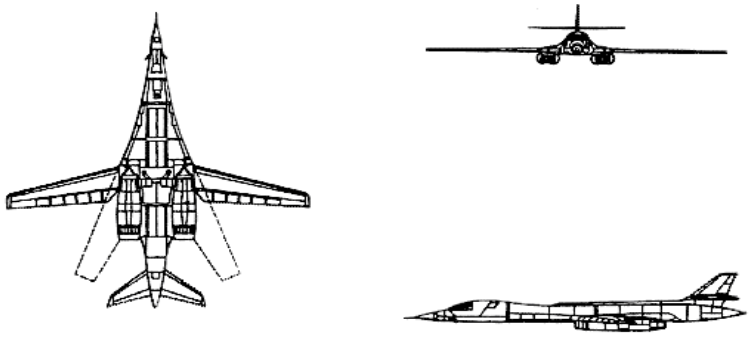

Figure 3: B-1B Lancer

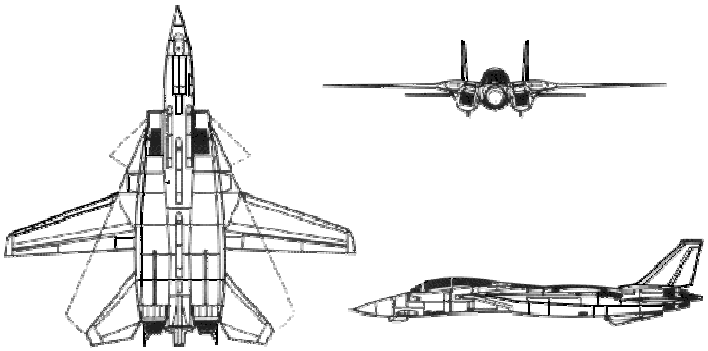

Figure 4: F-14 Tomcat

The F-14 Tomcat, shown in figure 4 is a “supersonic, twin-engine, variable sweep wing, two-place fighter designed to attack and destroy enemy aircraft at night and in all weather conditions” [11]. The wings are shoulder-mounted and are programmed for automatic sweep during flight, with a manual override provided. Normal sweep range is 20° to 68° with a 75° "oversweep" position provided for shipboard hangar stowage; sweep speed is 7.5 degree per second. For un-swept, low-speed combat maneuvering, the outer 2 sections of trailing edge flaps can be deployed at 10° and the nearly full-span leading-edge slats are drooped to 8.5°.

2.1.2 Variable Cambered Wings

Variable camber devices are mechanisms that allow for a change in airfoil curvature. Essentially, this geometry change can allow for roll, yaw and pitch control as well as improving aerodynamic performance. The Wright Flyer employed this technique in the

form of wing warping to control roll. The R. B. Racer, created by the Dayton Wright Airplane Company may be an example of the earliest use of variable camber in the context of performance morphing [12]. A manual hand crank was used to increase camber during take-off. Once airborne, the pilot could decrease the camber to improve aerodynamic efficiency and speed. More recent examples of morphing, variable curvature wings include the variable camber wing developed at The University of Maryland [26] and the NASA Dryden inflatable wing [14]. Flaps, slats and slots are standard variable camber devices [4].

Maryland Variable Camber Wing

Researchers at The University of Maryland have designed and developed a model of a multi-section variable camber wing [13]. This model is shown in figure 5. The NACA 0012 airfoil provides the baseline model for this wing. Each airfoil rib is divided into six sections, and has the ability to rotate up to 5° with no significant discontinuity to the wing surface. The wing is morphed via pneumatic actuators located at the main spar. Up to 10% change in camber is achieved. Wind tunnel tests indicate that the lift produced by the variable camber wing compares favorably with that of a solid wing in the same configuration.

However, this wing generates more drag than a baseline wing of the same dimensions due to skin friction. This is because a rigid wing can employ a single rigid skin, while the cambered wing skin needs to be flexible to accommodate rotation of the rib sections.

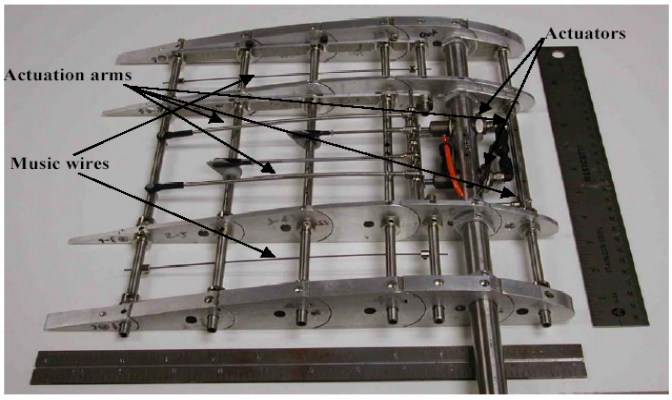

Figure 5: Variable Camber Wing

NASA Dryden Inflatable Wing

NASA Dryden has developed an inflatable wing whose curvature changes in response to an input of pressure [14]. As shown in figure 6, pressurized tubular structures provide definition to and support of the aerodynamic loads of this wing. Wind Tunnel tests conducted at the NASA Dryden Flight Research center indicate that the aerodynamic behavior of the inflatable wing compares satisfactorily to that of a solid wing of similar dimensions.

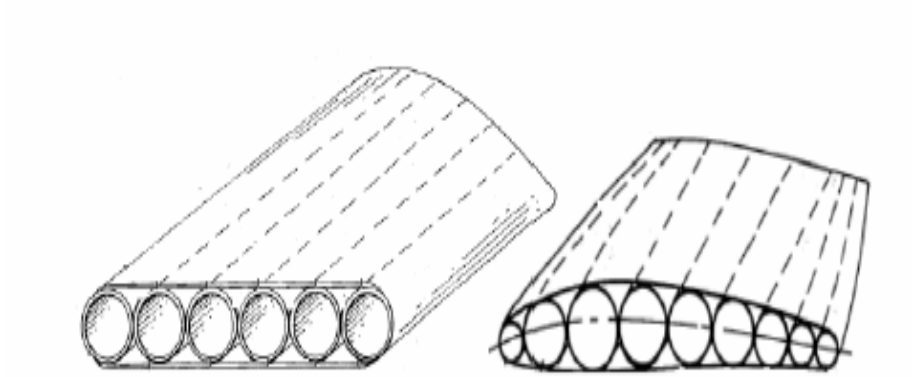

Figure 6: NASA Dryden Inflatable Wing in (a) baseline and (b) inflated states

High Lift Devices

Flaps, slats and slots are high lift devices that meet the need for improved performance during take-off and landing. The simple flap or aileron is the most common of these devices. Rotation of the aileron effectively changes the camber of the airfoil, consequently changing $C_{L_{\max}}$, the maximum lift coefficient, and $\alpha_{L=0}$, the zero-lift angle of attack. Slats are elements mounted on the leading edge of a wing at an orientation that essentially delay stall at the leading edge. Together with flaps they serve to maintain laminar flow over the wing. With these devices, the stall velocity can be sufficiently decreased during straight and level flight, steeper descents can be achieved during landing without an inordinate increase in airspeed, and the ground roll during takeoff is decreased. The actuation of high lift devices involves bulky control mechanisms. These devices tend to incur significant drag penalties.

2.1.3 Variable Span Wings

Proposals for telescoping wing technologies can be found as early as the 1940's. However, there is little evidence that any of these devices has ever been built. More recently, in 1997, the GEVERS AIRCRAFT INC. designed a variable span-telescoping wing for use on a 6-seat triphibious aircraft [15]. This aircraft is shown in figure 7. When retracted, the wing is capable of high speed cruise. Furthermore, enhanced low-speed performance is achieved when the wing is extended.

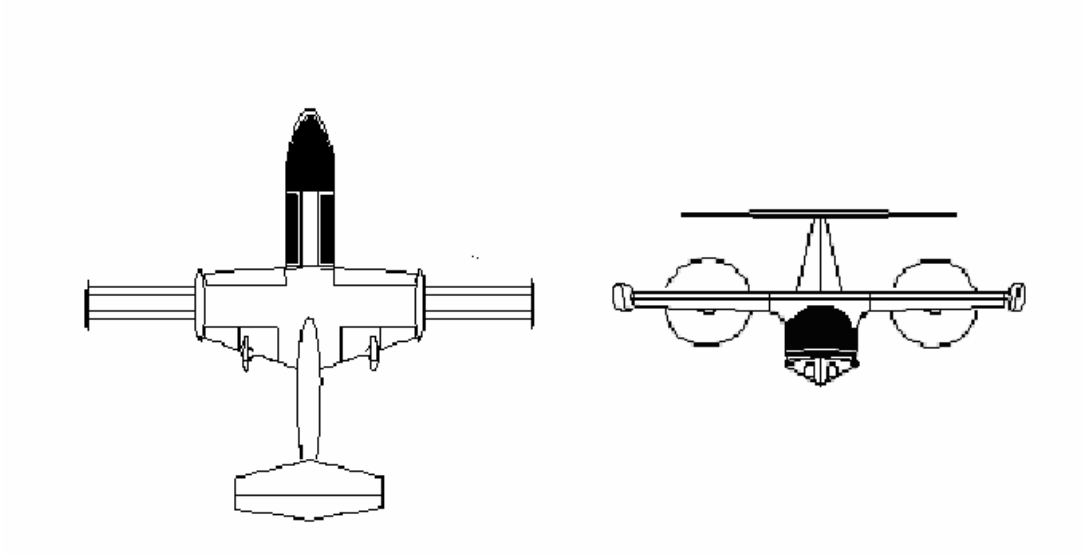

Figure 7: Gevers Variable Span Aircraft

2.2 State of the Art in Roll Control

The first practical application of a morphing technology was implemented on the Wright Flyer [16]. Wilbur Wright's study of the flight of birds led him to conclude that birds "regain their lateral balance when partly overturned by a gust of wind by torsion of the wing tips" [16]. This concept, coined "wing warping", involves twisting and bending the entire wing in order to control rolling motion. It was successfully tested by the Wright brothers on a biplane kite, controlling it by means of four strings from the ground. When this concept was later implemented on their powered aircraft, the pilot used cables to pull on the wings to change their shape, so enabling control and maneuvering of the aircraft. Conventional roll control and morphing roll control are discussed in the subsequent sections.

2.2.1 Conventional Roll Control

Most modern, conventional aircraft use either ailerons or spoilers to control lateral dynamics. Ailerons provide the primary means of lateral control on most modern aircraft. Their genesis is the subject of some debate [17]. The first prescience for roll control appeared in a concept for ailerons patented in 1868 by the Briton, M. P. W Boulton [17]. At that time, no practical aircraft existed on which to demonstrate his idea, so relegating the invention to oblivion. Nevertheless, Boulton only appreciated the rudimentary principle behind roll control. Indeed, the method of aileron construction outlined in his patent would have resulted in capsizing the aircraft [17].

In 1870, Richard Harte patented a concept for flap-type ailerons on a fixed-wing tractor airplane [17]. This device was conceived as a means of:

1. "Exercising control in roll to offset propeller torque"
2. "As elevators"
3. "As steering air-brakes"

However, Harte did not perceive this device for roll control per se. Both devices patented by Harte and Boulton were soon lost to oblivion.

In his book, *La Locomotion Aérienne* (1884), the Frenchman M. A Goupil presented a design for a monoplane. In the book, he describes two elevons that were mounted on the fuselage ahead of the wings. The primary function of these surfaces was to control pitch in liaison with the horizontal moveable tail. Secondarily, Goupil perceived these elevons to act as ailerons in controlling roll. Since Goupil had not envisioned the ailerons as

functioning in sync with rudder action, his machine probably would have been futile in roll control had his design ever been built and tested.

The year 1904 saw the first use of ailerons in a test flight. Frenchman Esnault-Pelterie used aileron-type surfaces instead of warping on his version of the 1902 Wright Glider [17]. His machine, however, was a failure and Peltetrie did not conduct any subsequent experiments to modify and improve his machine.

In 1905, the expatriate American, S. F. Cody built and flew a biplane kite glider that was fitted with ailerons similar to the type used earlier by Esnault-Pelterie [17]. Cody's glider was doomed to failure because of its non-rigid wing surfaces and inadequate flight control.

The true precursor of the modern-day aileron first appeared on Henri Farman's 1909 biplane, the *Henri Farman III.* Wing warping, the traditional form of roll control until then, was abandoned as most designers adopted Farman's design.

In addition to changing the total lift on each wing, aileron deflection is accompanied by a change in the drag on each half wing. The profile drag on each half wing increases in response to aileron deployment. Induced drag increases on the wing with positive aileron deployment (trailing edge down), whereas there is a decrease in induced drag on the wing with trailing edge up. The consequence of this variation in drag is an effect known as adverse yaw. If both ailerons are deflected by the same amount the profile drag does not

contribute to the adverse yaw [18]. Adverse yaw can be alleviated by the use of frise ailerons or differential ailerons.

Aileron Spoilers and Jet Spoilers

An aileron spoiler is a device mounted on the upper surface of an airfoil. This type of device is shown in figure 8. When extended into a flow, it forces boundary layer separation. The resulting decrease in lift on the wing on which the spoiler is deployed can be used to generate a roll moment. Roll control can be achieved by the use of spoilers installed on the outboard section of a wing. Spoilers always produce a favorable

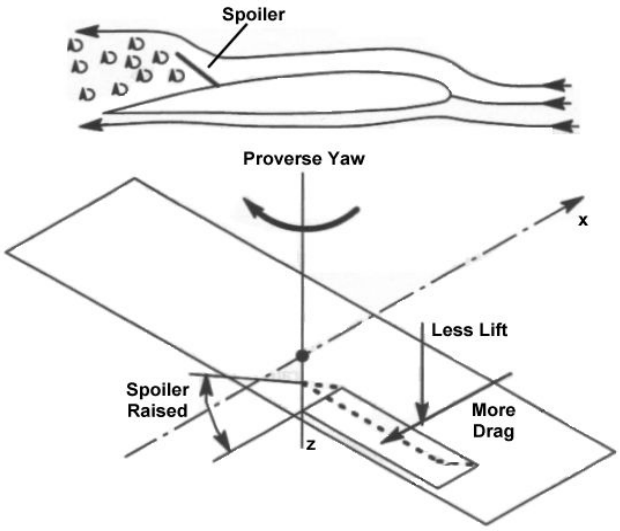

Figure 8: Operation of Aileron Spoiler

yawing moment because of the drag increase that accompanies spoiler deployment. It should be noted that the method of spoiler deployment is different from that of ailerons. When ailerons are used for roll control, both ailerons are deflected asymmetrically with respect to each other. However, roll control is accomplished via the protrusion of a

single spoiler into the flow. The use of spoilers for roll control may not always be a viable option. A classical objection to the use of spoiler ailerons is the altitude decrease that accompanies the loss of lift. Spoilers demonstrate nonlinear characteristics at low aileron projections and may even become ineffective at high angles of attack. In addition to this, there can be a delay in the resumption of an attached flow pattern after spoiler retraction. Pictures of typical spoiler ailerons are shown in Figure 9.

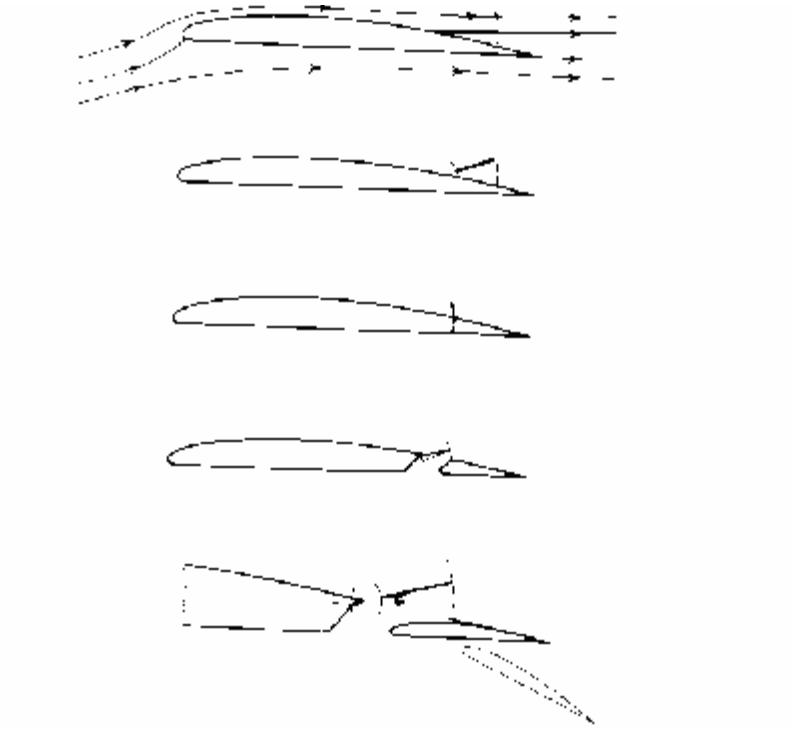

Figure 9: Aileron Spoilers

The motivation for early research into the use of spoilers for roll control was two-fold:

1. The need to negate adverse yaw (accompanied by the use of ailerons for roll control)
2. The need for adequate control post-stall and at high lift coefficients

Spoilers have been used for roll control since the 1930's. In 1932, Weick and Wenzinger conducted extensive wind tunnel tests in order to assess the use of spoilers [19]. In 1934, Weick, Soulé and Gough ran comprehensive tests on the use of spoilers on the *Fairchild 22* [19]. The year 1936 saw extensive tunnel and flight-testing of spoilers by the Germans [19]. The purpose of these tests was to realize an appropriate method for spoiler roll control on the *Messerschmitt ME 109.*

Despite the intensive research, spoilers did not become a popular method of control until the next decade. The discovery of the aileron reversal phenomenon and the emergence of sweepback ushered in the contemporary use of spoilers for control. Almost all jet transports use spoilers for supplementary roll control, especially at high speeds when outboard ailerons are locked out. The Grumman F11F-1F, A-6A, North American A-5A, and the General Dynamics/Grumman F-111 are examples of the use of spoilers by the military.

Jet Spoilers

Recent research has demonstrated that, in light aircraft, roll can be controlled by inserting pressurized air into a single wing's boundary layer [20]. The conduit for the pressurized air insertion is a jet spoiler. Figure 10 illustrates this effect.

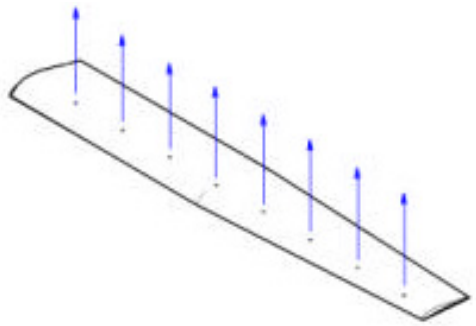

Figure 10: Jet Spoiler

Researchers at the Massachusetts Institute of Technology are exploring the use of jet spoilers to control roll on the Wide Area Surveillance Projectile (WASP) [20]. The WASP is a "folded UAV that a standard, 155-mm artillery round deploys as cargo" [21].

Figure 11: Wide Area Surveillance Projectile (WASP)

Due to the nature of its deployment, the WASP experiences forces on the order of 16,000-gs; this requires that its structure be g-hardened. The use of ailerons becomes

problematic because of this, as well as other limitations posed by actuators and manufacturing techniques.

The ideal jet spoiler was approximated by a span-wise row of pressure ports; a set of pressure ports was placed at both the 25% and 45% chord-wise location. Testing was conducted at the Wright Brothers Wind Tunnel at 60mph through angles of attack of –2 ° until stall (16°). The spoiler on each wing was tested at static and ram air conditions with spoiler pressures from 0-0.45 pound per square inch gage (psig). No effect was observed for this spoiler. However, the spoiler at 25% chord demonstrated an observable effect, generating some 2 inch-pounds of roll moment.

2.2.2 Morphing Roll Control

Variable Twist and Variable Curl Wing

Researchers at the University of Florida have developed a fleet of Micro Air Vehicles (MAVs) [22]. The airframes of these vehicles are constructed from carbon fiber, with wings made from flexible membrane sheeting. Morphing was considered as a control effector on two of these vehicles [23]. These vehicles are shown in figures 12 and 13. The 24-in span vehicle shown in figure 12 was considered for symmetric morphing. Roll control on this vehicle was investigated by using torque rods to twist each wing.

These rods lie along the span of each wing and are actuated by servos mounted inside the fuselage. Separate commands to each rod control the morphing.

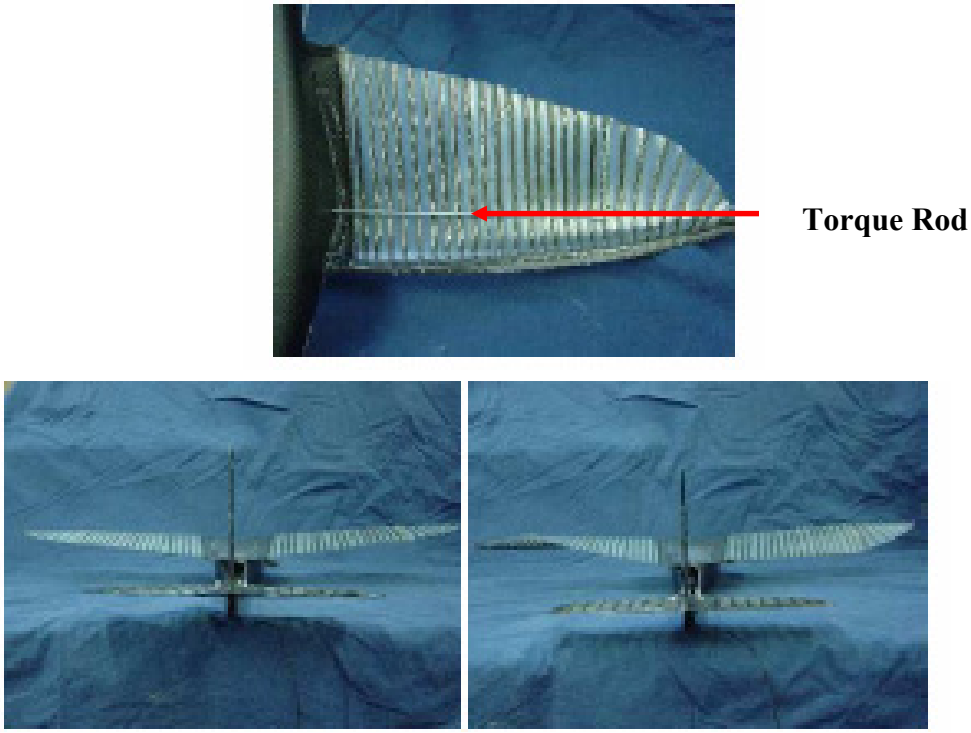

Figure 12: Symmetric Morphing on 24-in Span Vehicle

The vehicle was mounted with a data acquisition card (DAQ), 3-axis gyro and accelerometer. Morphing commands of varying magnitudes and durations were commanded after the aircraft was trimmed for straight and level flight. These commands consist of a constant left deflection for a certain time period followed immediately by a right deflection for the same time period and finally returning to trim [23]. Small maneuvers were performed about trim enabling a linear model to be extracted from the data.

Data from flight tests were used to approximate a linear time domain model for the lateral dynamic motion of this vehicle. This method of model determination is known as system identification [24]. The roll and yaw rates obtained from this model compared favorably with the rates obtained experimentally. Roll rates obtained from morphing are significantly higher than the yaw rates. This indicates that almost pure roll motion is achieved with little coupling between roll and yaw. Rudder inputs were also considered for lateral control. Morphing roll rates were considerably greater than rudder roll rates; in addition to this, morphing inputs resulted in almost pure roll motion whereas rudder inputs tended to excite Dutch roll dynamics resulting from strong coupling between roll and yaw.

The 12-in vehicle shown in figure 14 was considered for asymmetric morphing. The wings of this vehicle are constructed from latex sheeting which is a more flexible membrane. The use of latex enabled more dramatic shape changes to be considered beyond basic twisting. Morphing on this vehicle involved variations in twist, span, camber and chord. For asymmetric morphing, torque rods are replaced by Kevlar threads as shown in figure 13. These threads are activated by rotary actuators mounted inside the fuselage, which also accommodated a 3-axis gyro, accelerometer and data logger. Morphing on this vehicle involved curling one wing and leaving the other in an undeflected configuration. The resulting increase in angle of attack and incidence angle on the curled wing results in a lift differential between both wings. As a result of this, a commensurate roll moment is created so inducing a roll rate.

Flight tests demonstrated significant roll rates in response to morphing doublets applied about a trim condition at steady level flight. Coupling between pitch rate and the lateral dynamics was also observed. The linear model obtained for the symmetrically morphed 24-in vehicle was also applied to the asymmetric 12-in vehicle. The simulated response obtained from the linear flight model does not fully agree with the actual experimental response. This is a consequence of the nonlinearity introduced by asymmetric morphing. It was concluded that morphing on this MAV was "suitable for commanding turns and correcting attitude perturbations…. Roll controllability was satisfactory throughout the airspeed range encountered during cruise, high speed dives, landing and approach" [23].

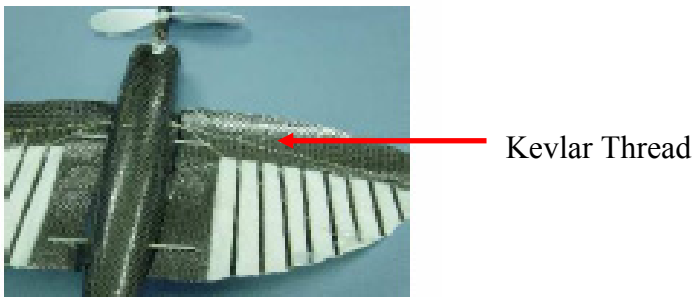

Figure 13: Kevlar Threads on Underside of 12-in MAV

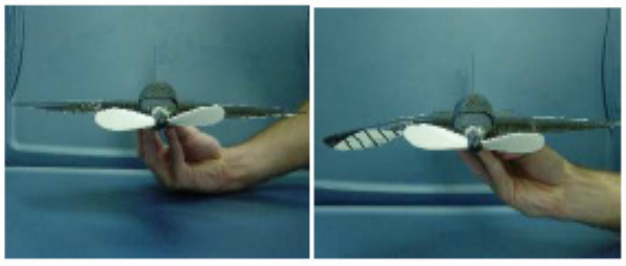

Figure 14: 12-in MAV in Undeflected and Asymmetrically Morphed States

Hyper Elliptic Cambered Span Wing

Researchers at NASA Langley have developed The Hyper-Elliptic Cambered Span (HECS) Morphing Wing for investigation into roll and yaw control [25].

The geometry of the wing is modeled by "a hyper-elliptic function in leading edge and trailing edge sweep and span-wise curvature" [25]. As seen in figure 15, a hingeless, morphable panel located at the trailing edge is used for roll and pitch control while a continuous morphable wing tip controls roll and yaw. A nonlinear CFD-based model was developed to analyze the stability and control properties of a vehicle incorporated with the HECS wing. The open loop lateral-directional dynamics of such a vehicle are shown to be unstable. However, stability augmentation via a closed loop controller demonstrates that the morphable panels on the HECS are a viable option for maneuvering.

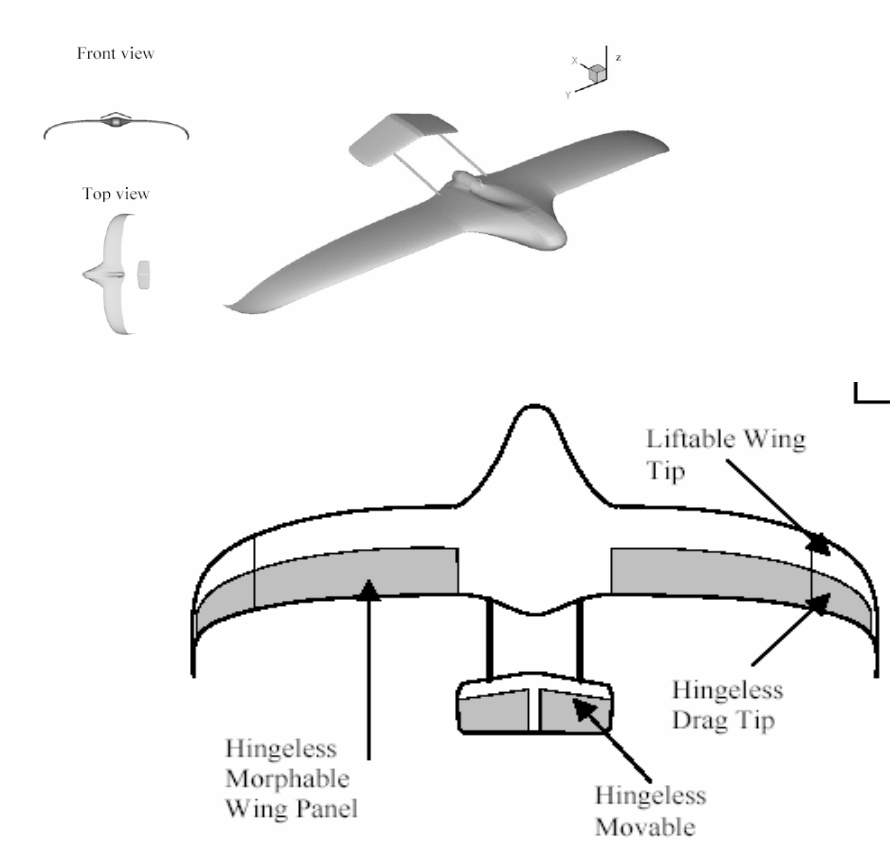

Figure 15: Hyper Elliptic Morphable Wing

This chapter has presented a survey of the state of the art in performance morphing and control morphing. The subsequent chapter describes how the Maryland variable span-morphing wing can be used to generate a roll moment. In particular, we examine and compare the theoretically predicted roll coefficients from VSWM with those from ailerons.

Chapter 3: Theoretical Prediction of VSMW Roll Moment

In this chapter we demonstrate theoretically that an aircraft using VSWM for roll control can produce roll coefficients that are equivalent to those obtained from aileron deflection. The variable span is the driving factor in creating an aerodynamic roll moment for the VSMW. Symmetric span configurations result in zero net moment. At any given pre-stall angle of attack, the total lift and total drag between each half wing differs as the span is varied asymmetrically. The resulting lift and drag differential give rise to a roll and yaw moment respectively. It is the roll moment that may be used to initiate a roll maneuver.

3.1 Finite Wing Theory Prediction

Finite wing theory is used to predict the roll moment coefficient for the asymmetric span configurations. The wing surface area, S and the lift curve slope, a, are both functions of span. In this section, we designate lift by the letter L and roll moment by the letter M. Note that in chapter 5, L signifies roll moment and M is used to mean pitching moment. The lift coefficient of a rectangular wing is given by [9]:

$$C_L = \frac{L}{q_\infty S} \tag{3.1.1}$$

where:

$$S = bc \tag{3.1.2}$$

$$C_L = a\alpha \tag{3.1.3}$$

$$a = \frac{a_0}{1 + a_0/(\pi AR)} \tag{3.1.4}$$

$$AR = \frac{b^2}{S} \tag{3.1.5}$$

By definition, the roll moment coefficient Cl is expressed as:

$$Cl = \frac{M}{q_\infty Sc} \tag{3.1.6}$$

Morphing was implemented as follows: the total symmetric wingspan was fixed at $b_0 = 2b_{sw}$. The starboard span, b_{sw} was then held fixed while the port wing span b_{pw} was varied. Note that b_{sw} and b_{pw} are measured with respect to the fuselage centerline. The resulting moment due to lift differentials on port wing (*pw*) and starboard wing (*sw*) is given as:

$$M = \left(L\frac{b}{2}\right)_{pw} + \left(L\frac{b}{2}\right)_{sw} \tag{3.1.7}$$

Simple manipulation yields:

$$Cl = \left(\frac{C_L b}{2c}\right)_{pw} + \left(\frac{C_L b}{2c}\right)_{sw} \tag{3.1.8}$$

Figure 16 illustrates these results. Define the variable on horizontal axis as: percentage change in span $\equiv \left(\frac{b_{pw} - b_{sw}}{b_{sw}}\right) \times 100\%$

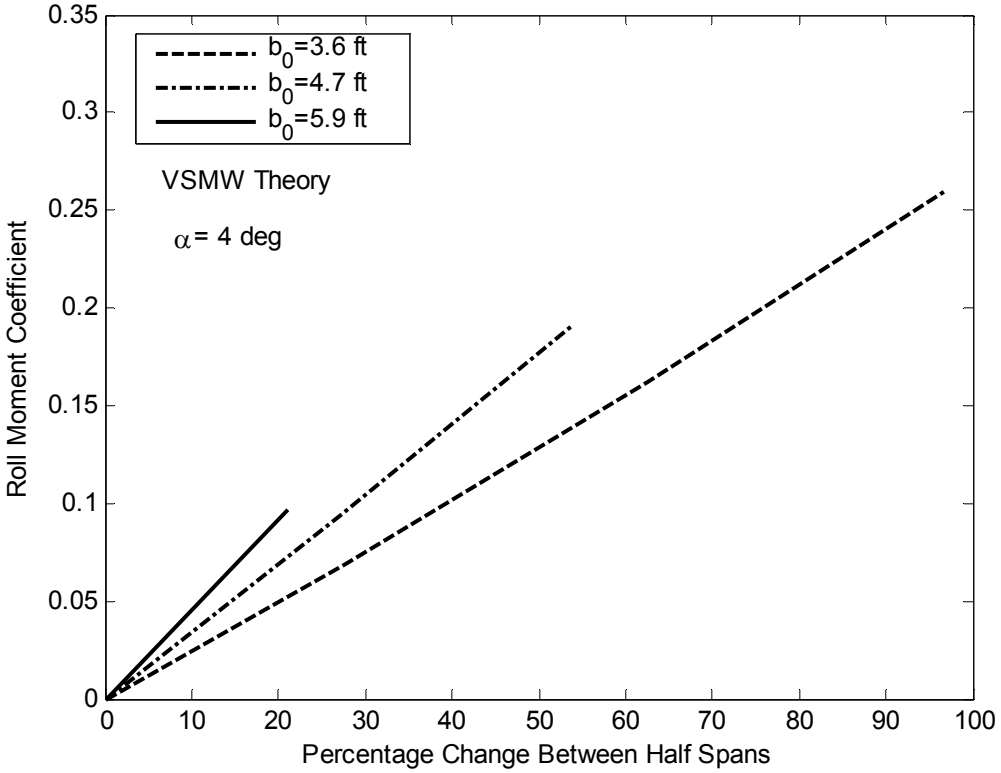

Figure 16: Theoretical Roll Moment from VSMW

There are two trends of interest in figure 16:

1. The roll coefficient varies linearly with percentage change between half spans from the symmetric reference condition.
2. As the total span, b_0 of the symmetric reference condition increases, the roll coefficient increases as well. This is a consequence of the larger moment arm and the increase in a, the lift curve slope

3.2 Comparison between Theoretical VSMW and Aileron Roll Coefficients

Ailerons are the traditional control effector of roll dynamics. Theoretical aileron roll coefficient data is presented for comparison with the variable span roll coefficients. The three symmetric spans used in the VSMW investigation are also used here. The sizing requirements for the ailerons were selected from historical guidelines outlined in reference [27]. An aileron chord to wing chord ratio $\frac{c_a}{c_a} = 0.12$ was selected. This ratio corresponds to a total aileron span to wing span ratio $\frac{b_a}{b_w}$ of approximately 1. The flap effectiveness factor τ, in equation (3.2.1) below is a function of $\frac{c_a}{c_w}$. The aileron chord to wing chord ratio of 0.12 corresponds to a τ of 0.4. An upper bound for the roll moment obtained from aileron deployment is given in reference [4]:

$$L = 2qa_0\tau\delta_a \int_{y_2}^{y_1} cydy \tag{3.2.1}$$

where:

$$\delta_a = \delta_L = \delta_R \tag{3.2.2}$$

A comparison between aileron and variable span coefficients is not entirely straightforward. For a high fidelity comparison one needs to develop a normalization method that accounts for the following: as an aileron is deflected, the sectional angle of attack changes; this is not true for variable span. Furthermore, aileron deflection does not change the total wing area. Clearly this is also not true for the VSMW.

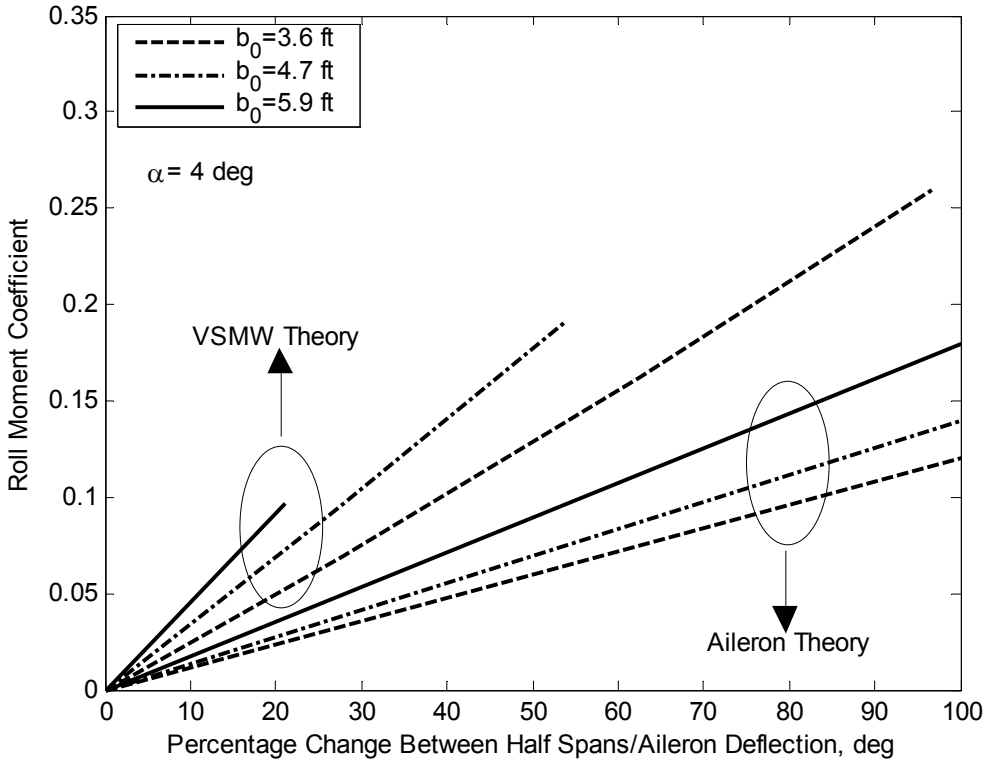

Figure 17: Comparison between Theoretical VSMW Roll Coefficient and Theoretical Aileron Roll Coefficient

This data is plotted in figure 17. Despite the fact that the data presented is not normalized, one can still draw some general conclusions. As expected, the VSMW is capable of producing roll coefficients that are equivalent to those obtained from aileron deployment. The maximum practical aileron deflection is about 25°. Observe however, that the VSMW can assume asymmetric span increases of up to 100%. Hence, its control authority can exceed that of the traditional aileron effector. Note that for a given aileron deflection, δ_{ail}, and some b_0, a small VSMW percentage change (from the same b_0) is required to achieve the same roll moment coefficient, *Cl*. In addition to this, for a fixed δ_{ail}, as b_0 increases it is clear that there is corresponding decrease in the equivalent VSMW percentage span increase.

Table 1 contains data that illustrates this more clearly. The data shown is given for the maximum practical aileron deflection of 25°. Consider the case where b_0=3.6 ft. This corresponds to a 10% VSMW percentage change. The same trends are seen for b_0=4.7 ft and b_0=5.9 ft. Note also that as b_0 increases, the corresponding VSMW percentage increase decreases.

Table 1: Data Showing Trends Illustrated in Figure 17

δ_{ail_max} **=25°**	**Maximum Aileron Roll Moment Coefficient**	**Corresponding VSMW Percentage Increase**
b_0=3.6 ft	0.028	10 %
b_0=4.7 ft	0.035	7.5 %
b_0=5.9 ft	0.045	5.5%

As one would expect, the center of gravity migrates along the *y*-body axis (span-wise) as the wing is morphed asymmetrically. Center of gravity displacements of up to two inches were observed when the Maryland VSMW was morphed asymmetrically. In this analysis, the moment due to the *cg* shift is ignored since it is smaller in magnitude than the aerodynamic roll moment.

Adverse yaw can be controlled by application of rudder. In particular, the yaw moment is expected to be small since the span differential required to create a roll moment is small.

In the following chapter we present the Maryland Variable Span Morphing Wing. We describe the mechanics of operation of the wing, its integration to a generic fuselage body, and wind tunnel tests on this generic wing-body model.

Chapter 4: Maryland Variable Span Morphing Wing

The purpose of this chapter is to describe the development of the Maryland Variable Span Morphing Wing and its mechanics of operation. In addition, we describe the integration of two half-wings to a generic UAV fuselage body, and wind tunnel tests on this wing body (WB) model. A comparison between theory and experiment is presented.

The main component of the VSMW wing is a pressurized telescopic spar that can undergo large-scale span-wise changes while supporting pressures in excess of 15 lbs/ft^2. NACA 0012 rib sections maintain the wing cross-section while telescopic skin sections preserve the span-wise airfoil geometry and ensure compact storage and deployment of the telescopic wing [26].

Wind tunnel testing was conducted on a generic wing-body (WB) model in the Glenn L. Martin Wind Tunnel at the University of Maryland. The primary purpose of these tests was to quantify the effect of differential span on the roll moment coefficients. Thirty tests were conducted, with more than half of them devoted to asymmetric span configurations. The changing span is the driving factor in creating an aerodynamic roll moment. Symmetric span configurations result in zero net moment. At any given pre-stall angle of attack, the total lift and total drag between each half wing differs as the span is varied asymmetrically. The resulting lift and drag differential give rise to a roll and yaw moment respectively. These roll moments may be used to initiate roll maneuvers.

In this chapter we present a brief description of the VSMW half-wing and the mechanics of its operation. We also describe the integration of two half-wings to a generic fuselage.

Wind tunnel data is presented and discussed. The experimental roll coefficients produced by the VSMW are compared with the theoretical VSMW and aileron roll coefficients.

4.1 Wind Tunnel Model Development

In this section a description of the variable span morphing wing (VSMW) and its operation is presented. The VSMW uses pneumatic actuators that permit a change in span while simultaneously supporting structural wing loads. The key element of the wing is a pressurized telescopic spar that can undergo large-scale span-wise changes while under loadings in excess of 15 $lbft^{-2}$. The wing cross-section is maintained by NACA 0012 rib sections, with telescopic skin sections to preserve the span-wise airfoil geometry and ensure compact storage and deployment of the telescopic wing [26]. The components of the VSMW are listed below.

1. Telescopic pneumatic spar and its extension/retraction control mechanism
2. Ribs fixed at the end of each section of the pneumatic telescopic spar
3. Wing skins that deploy and retract
4. Length proximity sensors
5. A pressurized air source with associated valving

The pneumatic telescoping wing under consideration in this paper has numerous advantages over conventional wing technologies, including weight, compactness, compliance tailoring and minimal moving parts [26]. The following section describes each element in detail.

4.1.1 The Pneumatic Actuator

The actuator consists of two pneumatic telescoping spars, developed by the Ergo-Help Company in Arlington Heights, IL. Each spar is mechanically coupled to the other by a rib at the tip of each section and one at the base of the of the root section as shown in figure 18. The use of two spars instead of one helps to prevent uncontrolled vibration and provides a greater area for application of pressure during actuation. Each spar has been designed to withstand loadings in excess of 15 $lbft^{-2}$. Neither spar can act independently of the other as they are both connected to the same pressure line.

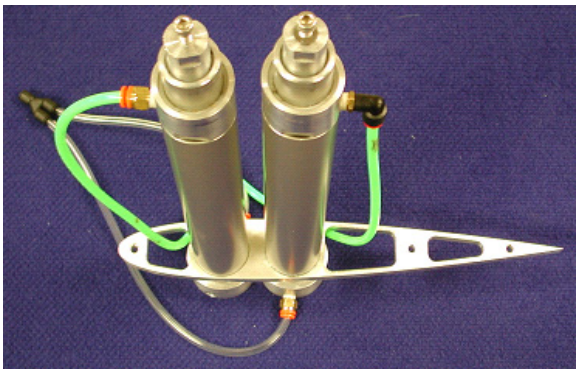

Figure 18: Ergo-Help Pneumatic Actuators

Figure 19 shows the details of the extension/retraction mechanism. An input of pressure at location (1) results in the extension of the middle (2) and tip element (3). Air is exhausted via orifice (4). Solenoid valves seal the input and output orifices when they are they are not being used. Consequently, the spars are always under pressure. In the retraction mode, pressure is fed to location (5), initiating the retraction of the middle element due to the force acting on area (6). Pressure escapes via orifice (7). The tip element remains fixed relative to the middle element until the latter has completely retracted. When the middle element is completely retracted, input of air at location (8) forces the tip element to retract with air escaping through (10).

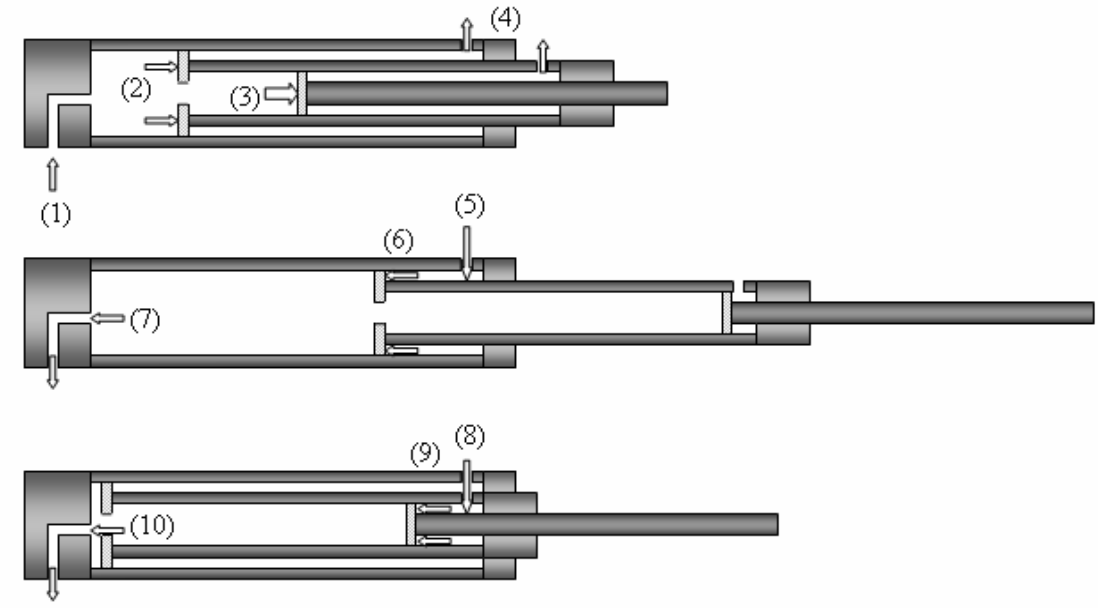

Figure 19: Ergo Help Pneumatic Spar Functional Design

4.1.2 Ribs

The rib section profiles were chosen so as to ensure ease of locating aerodynamic force data. Accordingly, the NACA 4-digit series was chosen as it is widely recognized and well understood. Furthermore, a symmetrical airfoil is desirable in order to facilitate theoretical predictions as well as manufacturing.

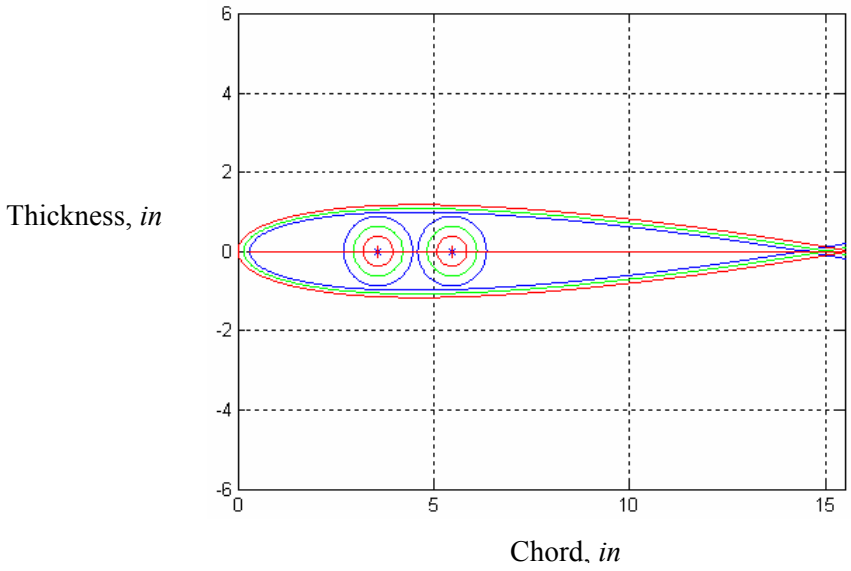

Figure 20: Variable Span Morphing Wing Airfoil Design

The smallest airfoil shape was designed using the NACA 0012 base equation and adapting the chord so that the two telescopic tube contours could be contained in it. The two larger shapes were designed to allow an even clearance of 0.060 inch everywhere around the smaller one. It is relatively easy to cut rib sections out of a 0.25 inch thick aluminum plate using a programmable milling machine. However, as shown in figure 21, each of them had to be manufactured in different ways to be attached at the right location

on the spar. The root section rib is slid on the two spars and rests on their attachment piece. The middle section rib was machined so that two screws can be used to tighten and solidly clamp the rib at the tip of the spars' middle section. The tip rib section was not completely extruded because it faces the exterior of the wing. However, some areas were carved to make it lighter, and two squared pockets were created to fit and attach to the end caps of the spars.

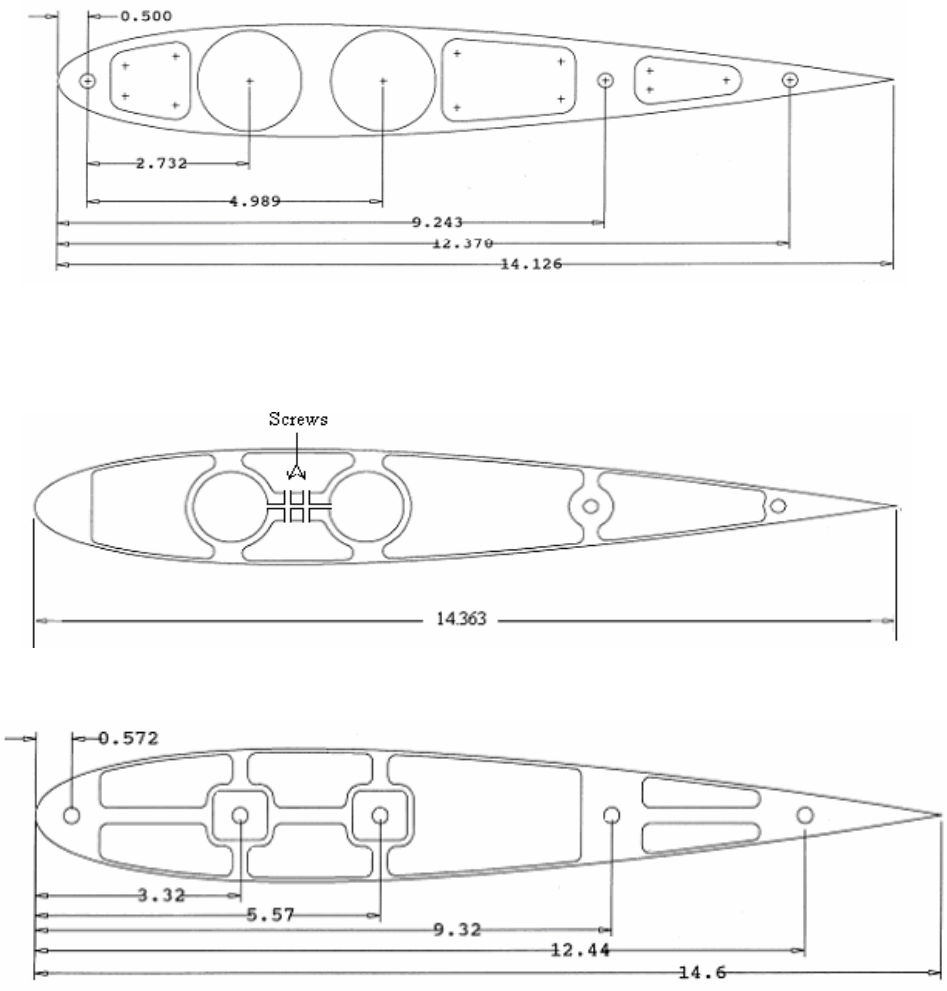

Figure 21: Rib Sections from (a) Root (b) Middle and (c) Tip Elements

4.1.3 The Skin

The skin consists of three hollow fiberglass shells of 0.045-in thickness. The use of a telescopic skin allows for several rigid sections to support aerodynamic loads while the wing is in any configuration. A rib was mounted at the tip of each moving section of the spar and at the tip and root of the fixed root section. The skins were then glued to the corresponding rib using epoxy. The fully integrated wing is shown in figure 22.

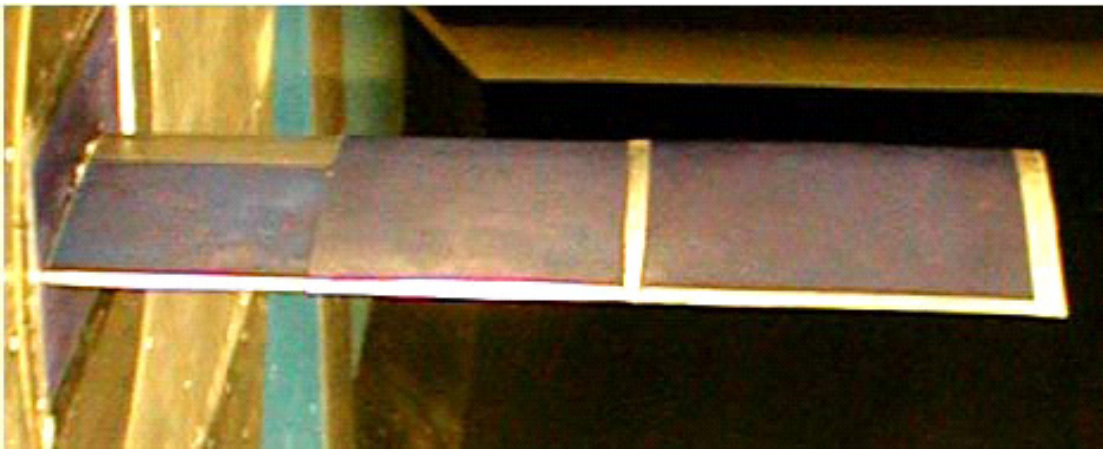

Figure 22: Fully Integrated Wing in Extended Configuration

4.1.4 Length Sensors

A 10-turn potentiometer mounted on a rack and pinion was chosen as the continuous sensing device. See figure 23.

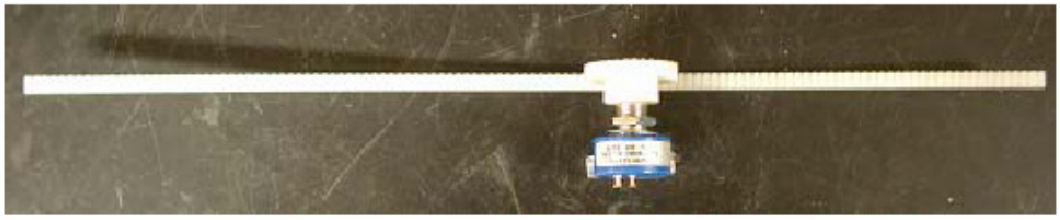

Figure 23: Potentiometer Mounted on Rack and Pinion

The 10-turn potentiometer was used to ensure a one-to-one correspondence between voltage and displacement. As illustrated in figure 24, both moving rib sections were mounted with a rack; the rack on each moving element was carefully aligned with the pinion on the lower rib. Figure 25 shows details of the mounting of the sensor (potentiometer on pinion) into the middle rib. Hence, the displacement of each moving section with respect to the fixed lower section can be sensed. The outputs from the two potentiometers were collected and transformed into a sum of displacements by a control program.

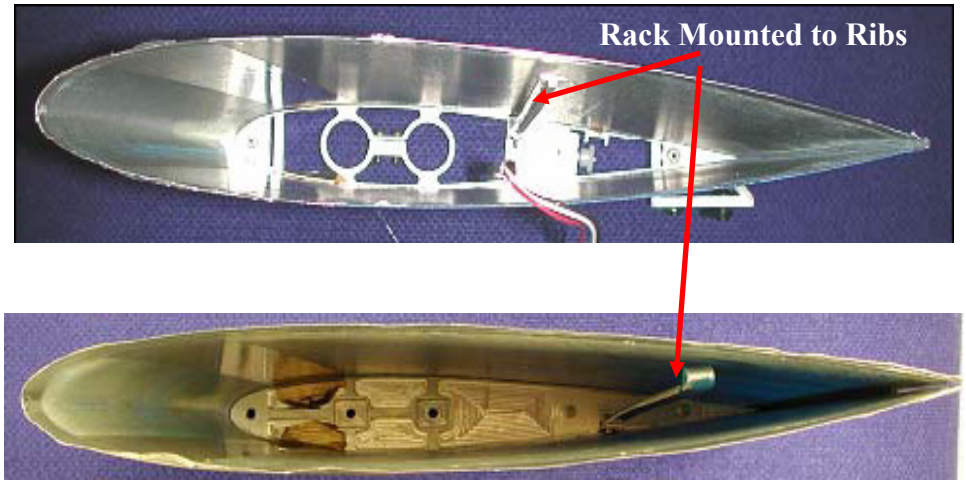

Figure 24: Integration of Rack into (a) Middle and (b) Tip Ribs

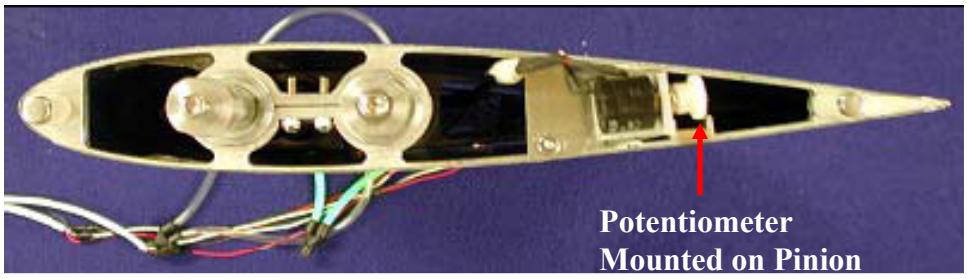

Figure 25: Middle Element Attachment and Sensor

4.2 Wing Body Integration

Two variable span half-wings were integrated to a generic fuselage body in order to perform wind tunnel tests. The wing-body (WB) model developed for wind tunnel testing is herein described. A very simple WB model was chosen. The fuselage was a hollow PVC cylinder, 71 inches in length with a 10.5-inch diameter. Each telescoping half-wing was mounted at a mid-wing location on an aluminum frame that had been specifically built for testing a variable sweep wing developed by a previous student. See figure 26 for details of the mounting apparatus. The frame was slightly modified to accommodate the variable span wing. The wing body interface was sealed with friction tape to ensure pre-stall laminar flow in this area. The pneumatic lines were fed through an orifice in the belly of the fuselage into a cavity in the wind tunnel floor and into the control room where they were attached to the compressor and electronic setup.

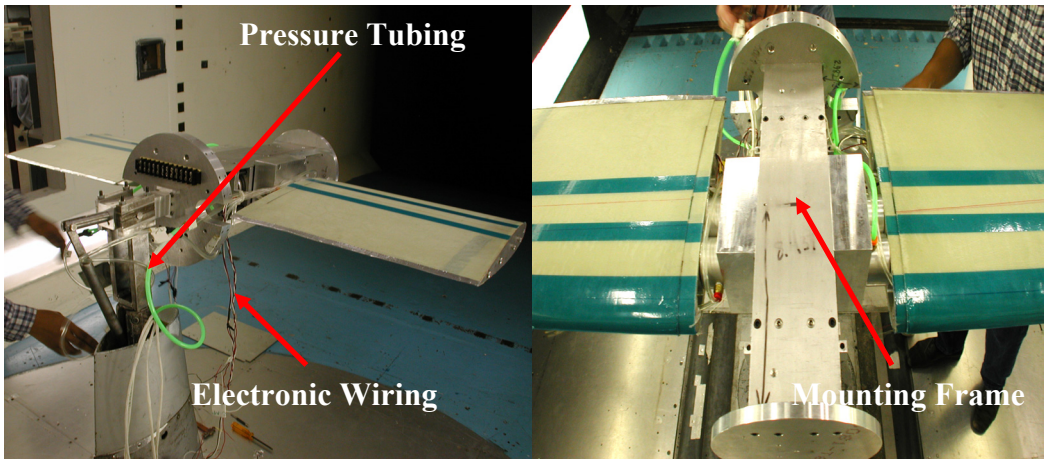

Figure 26 (a): Wing Body Integration

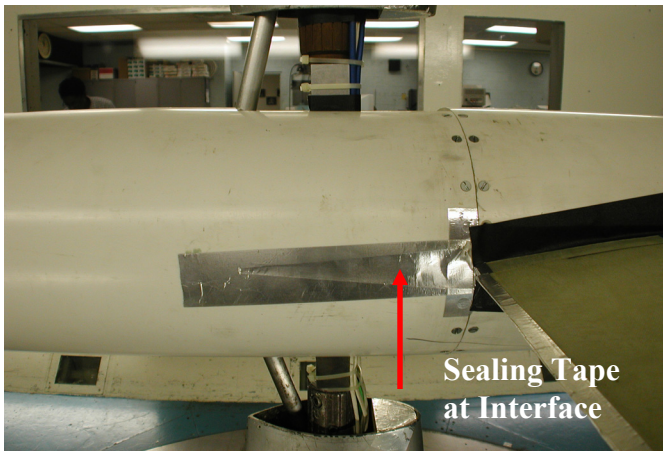

Figure 26(b): Wing Body Integration

4.3 Wind Tunnel Methodology

In December 2004, the wing-body model was mounted and tested in the Glenn L. Martin wind tunnel (WT) at the University of Maryland. See figure 27. The test section of the wind tunnel is 7.75 ft high x 11.04 ft wide with flow speeds ranging from 2mph to 230mph. The experiments were conducted on a six-component yoke type balance with the following component precision: Lift: 0.1 lbs, Drag: 0.05 lbs, Pitch: 0.1 ft-lbs, Yaw: 0.1 ft-lbs, Roll: 0.25 ft-lbs, Side Force: 0.1 lbs. The model was fully controllable from outside the tunnel as all the pressure lines and electronic wiring were passed through a cavity in the fuselage belly into the WT floor and out into the control room where they were connected to the compressor and electronic control system. The model was tested at free stream velocities of 20 mph, 25 mph and 30 mph at angles of attack from -2^{o} to 24^{o} at ten different span combinations. The test matrix is displayed in table 2.

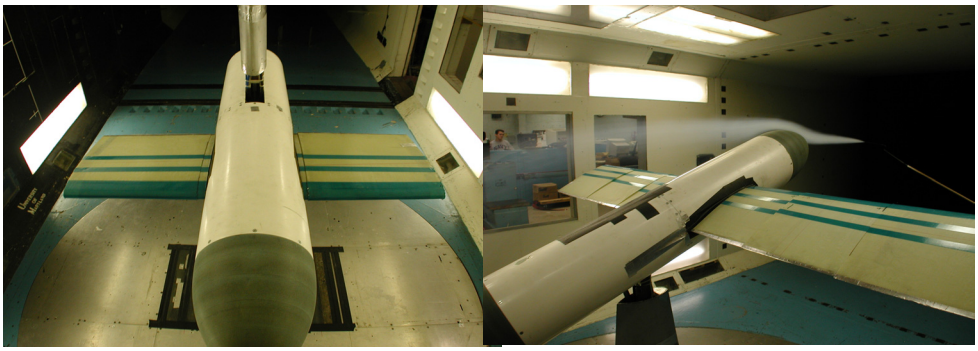

Figure 27: Wind Tunnel Tests of Wing Body Model in (a) Fully Retracted and (b) Fully Extended Configurations

Table 2: Test Matrix of Angles of Attack for given Airspeed and Wingspan Configuration

Test	Speed (mph)	AOA (degrees)	b_{0sw} (% span)	b_{0pw} (% span)
1	20- 30	0 to 24	40	40
2	20- 30	0 to 24	60	60
3	20- 30	0 to 24	80	80
4	20- 30	0 to 24	100	100
5	20- 30	0 to 24	40	60
6	20- 30	0 to 24	40	80
7	20- 30	0 to 24	40	100
8	20- 30	0 to 24	60	80
9	20- 30	0 to 24	60	100
10	20- 30	0 to 24	80	100

Morphing was implemented as follows: the total symmetric wingspan was fixed at $b_0 = 2b_{sw}$. The starboard span, b_{sw} was then held fixed while the port wing span b_{pw} was varied. This was carried out for three of the symmetric span configurations shown in the table 2. The 100-100 case was not included as only span *increases* from a symmetric reference condition were considered. Aerodynamic data on roll moment coefficients were thus obtained.

4.4 Aerodynamic Results

The variable span is the driving factor in generating roll moment. The wing surface area, S and the lift curve slope, a, are both functions of span. The lift coefficient of a rectangular wing is given by [9]:

$$C_L = \frac{L}{q_\infty S} \tag{4.4.1}$$

where:

$$C_L = a\alpha \tag{4.4.2}$$

$$a = \frac{a_0}{1 + a_0/(\pi AR)} \tag{4.4.3}$$

By definition, the roll moment coefficient C_l is expressed as:

$$Cl = \frac{M}{q_\infty Sc} \tag{4.4.4}$$

The resulting moment due to lift differentials on port wing (*pw*) and starboard wing (*sw*) is given as:

$$M = \left(L\frac{b}{2} \right)_{pw} + \left(L\frac{b}{2} \right)_{sw} \tag{4.4.5}$$

Simple manipulation yields:

$$Cl = \left(\frac{C_L b}{2c} \right)_{pw} + \left(\frac{C_L b}{2c} \right)_{sw} \tag{4.4.6}$$

Figure 28 illustrates the relationship between experimental and theoretical roll moment and changes in span. Define the percentage change in span as: $\left(\frac{b_{pw} - b_{sw}}{b_{sw}} \right) \times 100\%$. This represents an increase in span from a symmetric reference condition.

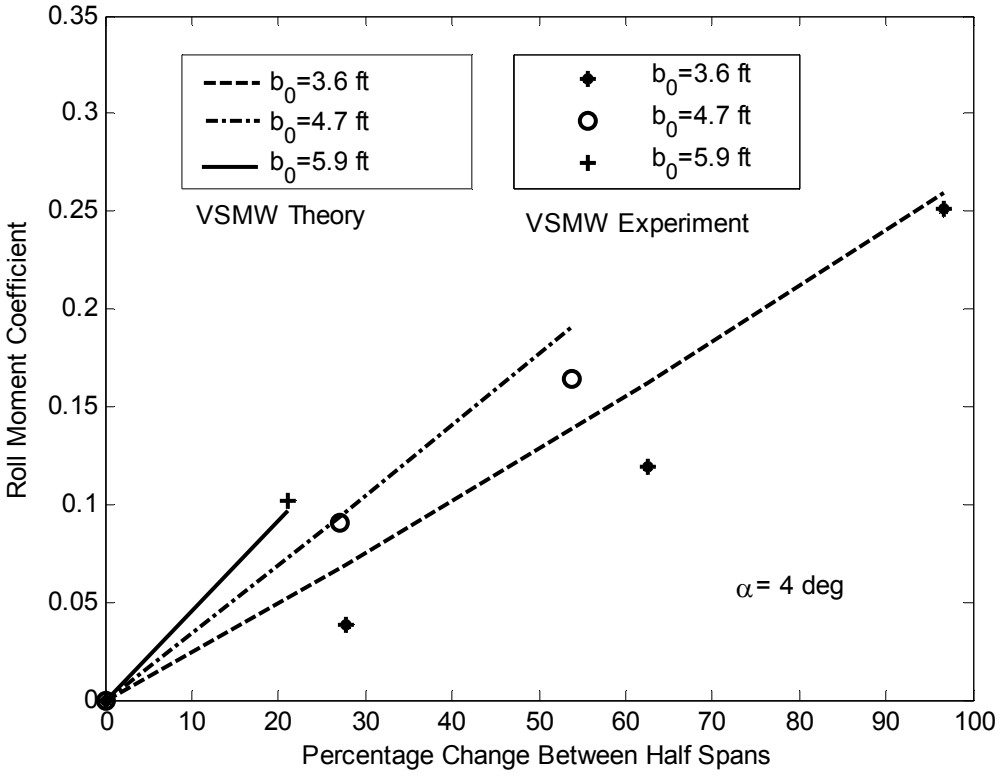

Figure 28: Theoretical and Experimental Roll Coefficient from VSMW

Two trends are illustrated in figure 28:

1. For b_0=5.9 ft and b_0=4.7 ft, the experimental data illustrates that the roll coefficient varies linearly with percentage change between half spans from the symmetric reference condition. The most retracted case, b_0=3.6 ft displays some nonlinear behavior which will be examined more closely.
2. As the total span, b_0 of the symmetric reference condition increases, the roll coefficient increases as well. This is a consequence of the larger moment arm and the increase in a, the lift curve slope

The experimental data corresponding to baseline spans of b_0=5.9 ft and b_0=4.7 ft show fairly good agreement with theory. As seen in figure 29, flow visualization tests indicate significant pressure losses, particularly at the seams. The study conducted in reference 26 indicates that these pressure losses affect the capacity of the wing to produce lift.

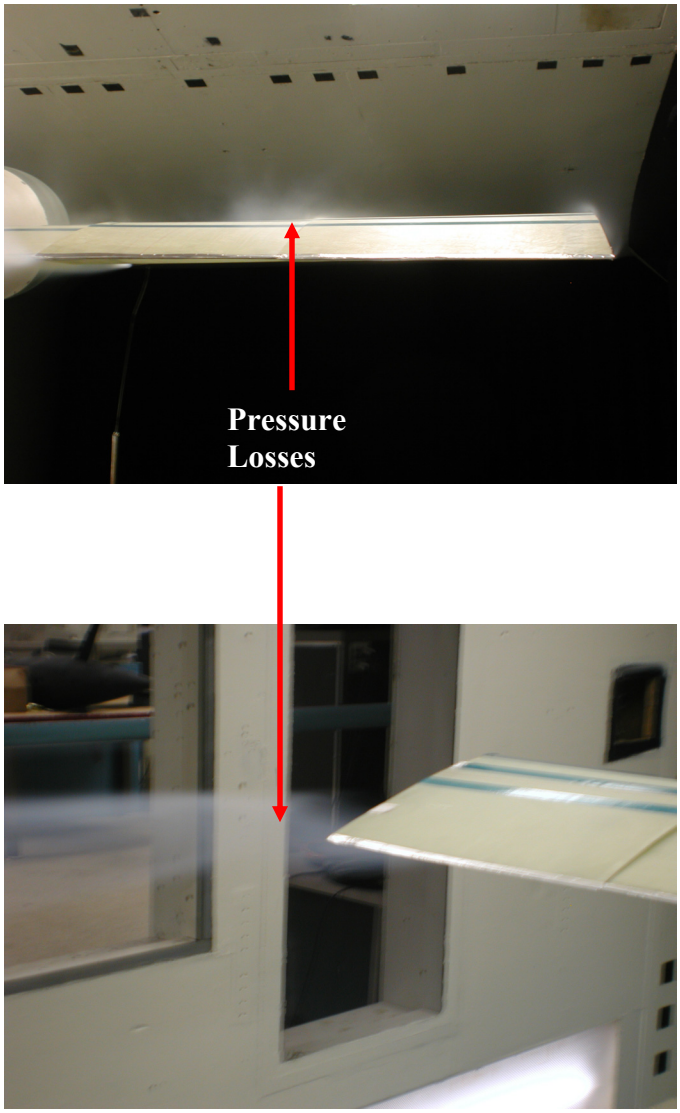

Figure 29: Flow Visualization of Pressure Losses at Seams and Tip

Since the roll moment is derived directly from the lift, it can be concluded that, for these two baseline cases, the discrepancy between theory and experiment is largely due to

pressure losses. One would expect pressure losses to increase as the baseline span b_0 increases.

However, pressure losses do not account for the discrepancy in the baseline case, b_0=3.6 ft. For this case, the experimental data display a trend that is clearly not linear. This case should have the least seam leakage and consequently the best agreement between experiment and theory. It appears as though the discrepancy in this case is due to an undesirable, nonlinear interference effect between the fuselage and wing. Observe that the half wing assumes a maximum value that is only about three times that of the fuselage diameter. See table 3. The close proximity of the wing tips to the wing-fuselage interface would serve to augment this interference effect. The half wing spans shown in table 3 are measured from the half wing root to half wing tip. Interference between the fuselage and the wing would affect the lift produced. This is verified by the results shown in table 4.

Table 3: Dimensions of Fuselage and Half Wing

Fuselage diameter	0.9 ft
40% Half Wing Span	1.4 ft
60% Half Wing Span	1.9 ft
80% Half Wing Span	2.5 ft
100%Half Wing Span	3.2 ft

Table 4: Lift Discrepancy for 40%-40% Baseline Case

Wing State	Theoretical Lift Coefficient	Experimental Lift Coefficient	Percentage Difference
40%-40%	0.27	0.10	62
40%-60%	0.28	0.12	61
40%-80%	0.30	0.15	49
40%-100%	0.31	0.21	30

It is not surprising that as the port wing half-span increases, (from 40% to 100%) theory and experiment show better agreement. Since the roll coefficient is derived directly from the lift coefficients one would expect the wing-fuselage interference effect to directly affect the roll coefficients.

Comparison with Aileron Roll Moment

Ailerons are the traditional control effector of roll dynamics. Theoretical aileron roll moment is presented for comparison with the variable span roll moment. The three symmetric spans used in the VSWM investigation are also used here. The sizing requirements for the ailerons were selected from historical guidelines outlined in reference [27]. An aileron chord to wing chord ratio, $\frac{c_a}{c_w} = 0.12$ was selected. This ratio corresponds to a total aileron span to wing span ratio, $\frac{b_a}{b_w}$ of approximately 1. The flap effectiveness factor τ, in equation (4.4.7) is a function of $\frac{c_a}{c_w}$. The aileron chord to wing

chord ratio of 0.12 corresponds to a τ of 0.4. An upper bound for the roll moment obtained from aileron deployment is given in reference [4]:

$$L = 2qa_0\tau\delta_a \int_{y_2}^{y_1} cydy \tag{4.4.7}$$

where:

$$\delta_a = \delta_L = \delta_R \tag{4.4.8}$$

It should be noted that in practice, ailerons are not usually deflected beyond 25°. However, the VSMW can undergo changes of up to 100%. Hence, the VSMW can produce roll coefficients that are equivalent to, and even greater than those from ailerons. Observe that due to the discrepancy between experiment and theory, a greater span

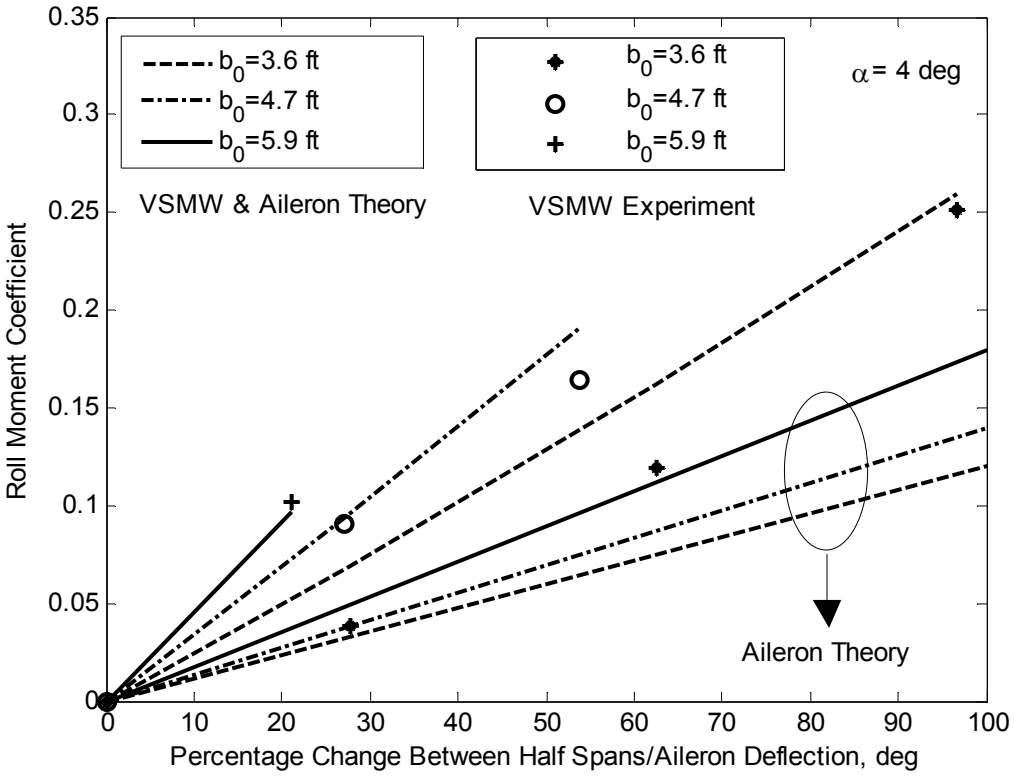

Figure 30: Comparison between Aileron and Span Roll Coefficient

increase is required to obtain an equivalent aileron roll coefficient.

The next chapter examines the details of the dynamic behavior of an aircraft with a VSMW. In particular, we revisit the 6-DOF model in order to derive the extra terms due to morphing. Application of the parallel axis theorem enables one to derive the ordinary differential equation that describes a steady roll induced by VSWM.

Chapter 5: Dynamics

In this chapter, the moment equations of the generic UAV model with the variable span-morphing wing are derived. The standard six-degree of freedom model that describes aircraft dynamics is revisited. In particular, we derive the extra inertial terms that morphing introduces into the 6-DOF model. These additional terms appear in the three moment equations with each moment equation containing seven additional terms.

It is well known that as any aircraft rotates the elements of its inertia matrix change relative to inertial space. To avoid this difficulty, it is standard procedure that the dynamic equations be given with respect to a body axis system that is fixed to and rotating with the aircraft. One should note however, that the geometry, and therefore the inertia matrix of aircraft with conventional controls also change with control position. These changes are routinely considered to be negligible. However, it is crucial to note that with a morphing vehicle, inertial changes still appear in the body axes. This is due to the variable geometry in body axes. The dynamic analysis of a morphing aircraft can be greatly simplified if one can develop simple expressions for these inertial changes.

One can establish simple expressions for these perturbations from the baseline moment equations by considering the case of a steady roll. Note the deviation in notation from that found in standard texts. In standard texts, perturbation terms correspond to a change in aerodynamic moment associated with a change in the state. In this work, we take perturbation terms to mean additional terms introduced into the dynamic equations by morphing. We show that for a steady roll, these perturbations are functions of δy, the

displacement of the center of gravity of the moving section, $\dot{\delta y}$, its time rate of change, m_s, its mass, and p, the aircraft roll rate.

In particular, we see that for a steady roll, morphing introduces an extra term into the well-known single degree of freedom model. The behavior of this term is that of modifying the damping in the system.

5.1 Derivation of Morphing Moment Equations

In this section we derive the complete morphing moment equations. Dynamic models of a morphing vehicle must account for the aircraft's variable geometry. As such, we retain the extra inertial terms that morphing introduces into the aircraft dynamics. Recall that

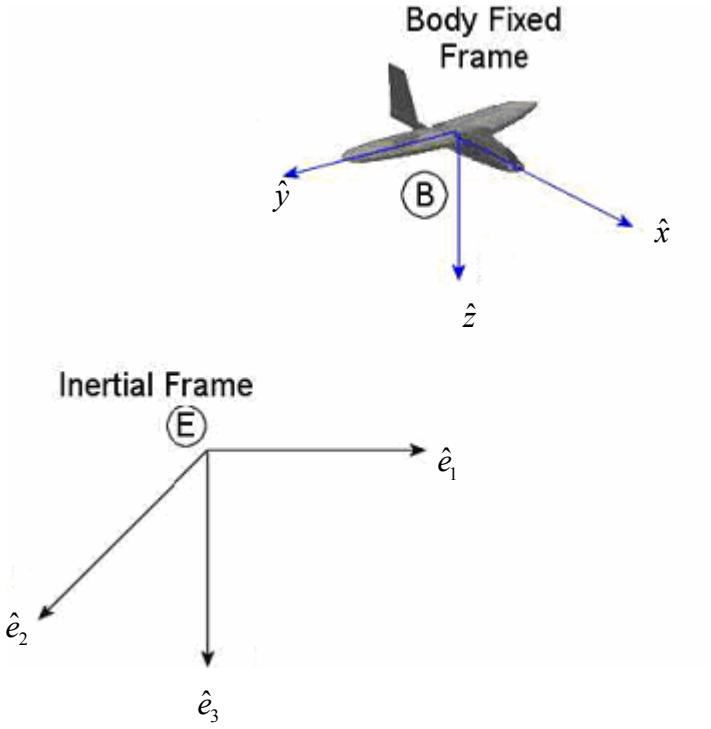

Figure 31: Body Fixed and Inertial Axis Systems

the body-fixed frame is fixed to and rotates with the aircraft, whereas the inertial frame remains fixed to the earth. See figure 31 for definitions of these coordinate frames. In this analysis we follow the development of baseline equations proposed in reference [28].

In this development we make the following assumptions:

1. The aircraft's total mass is constant, so that $\dot{\delta m} = 0$.
2. The earth's rotation relative to that of the aircraft is sufficiently small to justify the assumption that the earth is an inertial reference frame.

Moment Equations

The resultant moment, $\delta \mathrm{M}$, on an infinitesimal mass δm can be written:

$$\delta \mathrm{M} = \frac{d}{dt}\delta H = \frac{d}{dt}\left(r \times v\right)\delta m \tag{5.1.1}$$

$$\mathrm{M} = \sum \delta \mathrm{M} = \frac{d}{dt}\sum \delta H = \frac{d}{dt} H \tag{5.1.2}$$

where:

$$v = v_c + \frac{dr}{dt} = v_c + \omega \times r \tag{5.1.3}$$

$$H = \sum \delta H = \sum \left(r \times v_c\right)\delta m + \sum r \times \left(\omega \times r\right)\delta m \tag{5.1.4}$$

After expanding and assuming that $\sum r\delta m = 0$, the scalar components of (5.1.4) are expressed as:

$$\begin{aligned} H_x &= pI_x - qI_{xy} - rI_{xz} \\ H_y &= -pI_{xy} + qI_y - rI_{yz} \\ H_z &= -pI_{xz} - qI_{yz} + rI_z \end{aligned} \tag{5.1.5}$$

The moments and products of inertia in (5.1.5) above are defined as follows:

$$I_x = \sum (y^2 + z^2)\delta m$$
$$I_y = \sum (x^2 + z^2)\delta m \qquad (5.1.6)$$
$$I_z = \sum (x^2 + y^2)\delta m$$

Equations (5.1.5) are expressed in the inertial frame. One would like to take time derivatives of (5.1.5) in order to obtain the moments acting on the aircraft. Prior to this however, standard procedure requires that these equations be expressed in the body frame in order to eliminate time varying inertial terms. However, the changing geometry of a morphing aircraft requires that these time variant inertial terms be retained in the body axis system.

The relationship between the time derivatives of an arbitrary vector, *A*, in an inertial system *I*, and a rotating body system, *B*, is given by the theorem of Coriolis:

$$\left.\frac{dA}{dt}\right|_I = \left.\frac{dA}{dt}\right|_B + \omega \times A \qquad (5.1.7)$$

Applying (5.1.7) to (5.1.5) gives the components of M in body axis as:

$$L = \dot{H}_x + qH_z - rH_y$$
$$M = \dot{H}_y + rH_x - pH_z \qquad (5.1.8)$$
$$N = \dot{H}_z + pH_y - qH_x$$

After expanding, one obtains:

$$
\begin{aligned}
L &= \dot{p} I_x + p \dot{I}_x - \dot{q} I_{xy} - q \dot{I}_{xy} - \dot{r} I_{xz} - r \dot{I}_{xz} \\
&- qpI_{xz} - q^2 I_{yz} + qrI_z + rpI_{xy} - rqI_y + r^2 I_{yz} \\
M &= -\dot{p} I_{xy} - p \dot{I}_{xy} + \dot{q} I_y + q \dot{I}_y - \dot{r} I_{yz} - r \dot{I}_{yz} \\
&+ rqI_x - rqI_{xy} - r^2 I_{xz} + p^2 I_{xz} + pqI_{yz} - rqI_z \\
N &= -\dot{p} I_{xz} - p \dot{I}_{xz} - \dot{q} I_{yz} - q \dot{I}_{yz} + \dot{r} I_z + r \dot{I}_z \\
&- p^2 I_{xy} + pqI_y - prI_{yz} - qpI_x + q^2 I_{xy} + qrI_{xz}
\end{aligned}
\tag{5.1.9}
$$

These are the complete moment equations where additional terms due to morphing are retained. Recall that the left hand sides of equations (5.1.9) are the aerodynamic roll, pitch and yaw moments corresponding to the state and history of the state.

5.2 Separation of Moment Equations into Baseline and Perturbation Terms

The focus of this section is to use the parallel axis theorem to gain insight into the perturbation inertial terms. We can separate equations (5.1.9) into baseline terms L_0, M_0, N_0, and perturbation terms ΔL, ΔN and ΔM. Note here the deviation in notation from that found in standard texts. In standard textbooks, the expression "perturbation" refers to a change in aerodynamic moment associated with a change in the state. In this work, we define perturbation terms as additional terms introduced into the dynamic equations by morphing.

Define:

$$\begin{aligned} L &= L_0 + \Delta L \\ M &= M_0 + \Delta M \\ N &= N_0 + \Delta N \end{aligned} \tag{5.2.1}$$

where:

$$\begin{aligned} L_0 &= \dot{p} I_{x_0} - \dot{r} I_{xz_0} - qpI_{xz_0} + qrI_{z_0} - qrI_{y_0} \\ M_0 &= \dot{q} I_{y_0} + rq\left(I_{x_0} - I_{z_0}\right) + I_{xz_0}\left(p^2 - r^2\right) \\ N_0 &= \dot{r} I_{z_0} - \dot{p} I_{xz_0} + pq\left(I_{y_0} - I_{x_0}\right) + qrI_{xz_0} \end{aligned} \tag{5.2.2}$$

and:

$$\begin{aligned} \Delta L &= p\dot{I}_x - q\dot{I}_{xy} - q\dot{I}_{xy} - r\dot{I}_{xz} - q^2 I_{yz} + rpI_{xy} + r^2 I_{yz} \\ \Delta M &= -\dot{p} I_{xy} - p\dot{I}_{xy} + q\dot{I}_y - \dot{r} I_{yz} - r\dot{I}_{yz} - rqI_{xy} + pqI_{yz} \\ \Delta N &= -p\dot{I}_{xz} - \dot{q} I_{yz} - q\dot{I}_{yz} + r\dot{I}_z - p^2 I_{xy} - rpI_{xz} + q^2 I_{xy} \end{aligned} \tag{5.2.3}$$

Notice that $\Delta L, \Delta M$ and ΔN are the perturbation roll, pitch and yaw terms introduced by morphing. They do not appear in the moment equations for conventional fixed wing aircraft. These terms describe time varying inertias, time varying inertial products and pure inertial products. Note also that as discussed above, the baseline terms L_0, M_0, and N_0 do not contain time varying inertias of any kind.

Simplification of Perturbation Terms

By the Parallel Axis Theorem, define:

$$\begin{aligned} I_x &= I_{x_0} + m_s\left(y(t)^2 + z(t)^2\right) \\ I_y &= I_{y_0} + m_s\left(x(t)^2 + z(t)^2\right) \\ I_z &= I_{z_0} + m_s\left(x(t)^2 + y(t)^2\right) \\ I_{xy} &= I_{xy_0} + m_s x(t) y(t) \\ I_{xz} &= I_{xz_0} + m_s x(t) z(t) \\ I_{yz} &= I_{yz_0} + m_s y(t) z(t) \end{aligned} \tag{5.2.4}$$

where m_s is the mass of the *moving section* of the half wing. The coordinates of the center of gravity (*cg*) of the *moving section* with respect to the symmetric aircraft (A/C) *cg* location are given by *x(t), y(t) y(t).* Observe that the wing is restricted to changes in the *y* direction. Also notice that we assume that the A/C cg is fixed. Hence:

$$y(t) = y_0 + \delta y(t), \;\; x(t) = x_0 + \delta x(t), \;\; z(t) = \; z_0 + \delta z(t\;) \tag{5.2.5}$$

Note that only one half span of the full wing is being morphed while the other half span remains fixed. See figure 32.

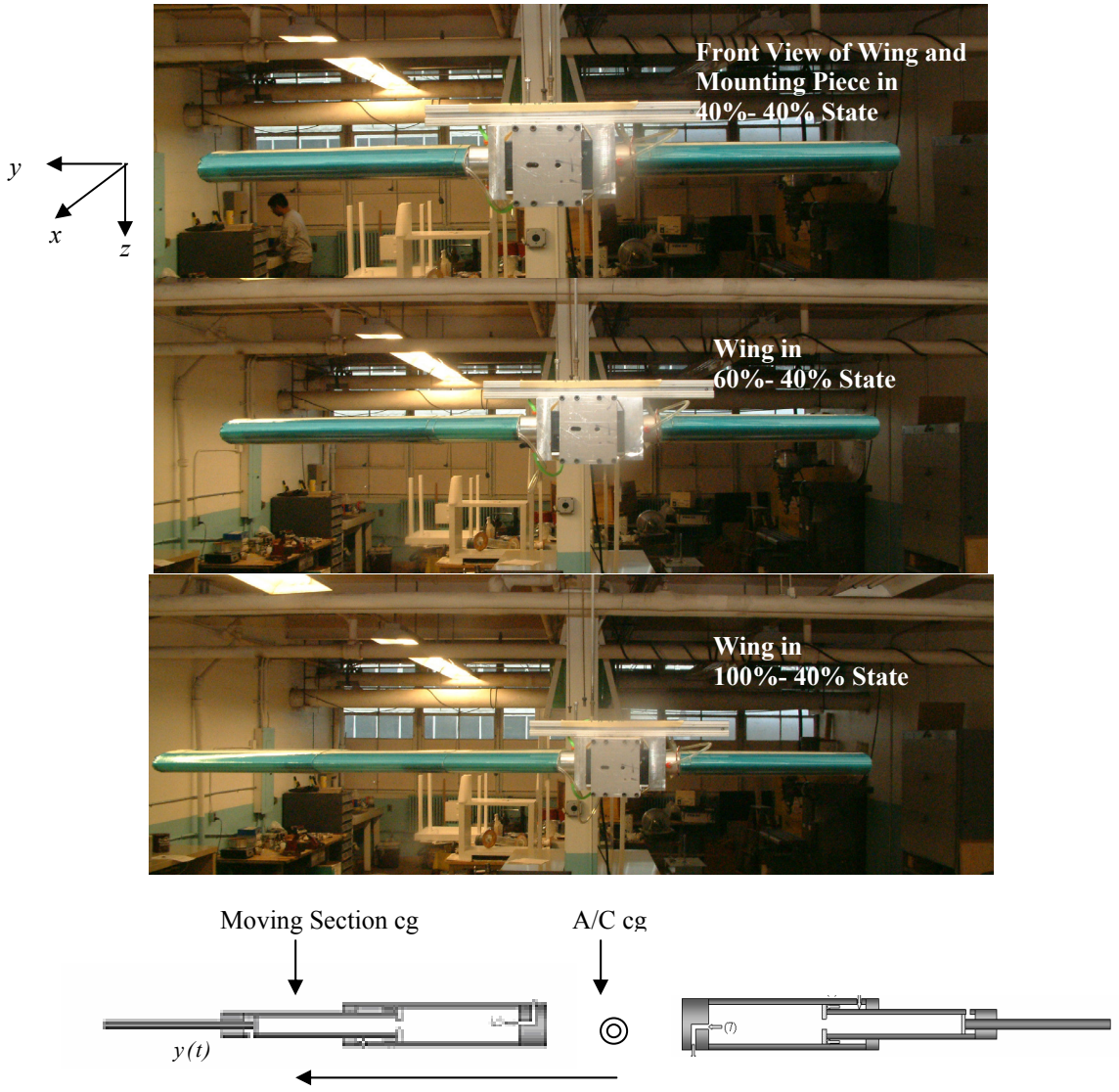

Figure 32: Sequence of Events during Asymmetric Morphing

Recall from (5.2.5):

$$\begin{aligned} x(t) &= x_0 + \delta x \\ y(t) &= y_0 + \delta y \\ z(t) &= z_0 + \delta z \end{aligned} \tag{5.2.6}$$

Taking derivatives of (5.2.4) with respect to time yields:

$$\begin{aligned} \dot{I}_x &= 2m_s\left(y_0\,\dot{\delta y} + \delta y\,\dot{\delta y} + z_0\,\dot{\delta z} + \delta z\,\dot{\delta z} \right) \\ \dot{I}_y &= 2m_s\left(x_0\,\dot{\delta x} + \delta x\,\dot{\delta x} + z_0\,\dot{\delta z} + \delta z\,\dot{\delta z} \right) \\ \dot{I}_z &= 2m_s\left(x_0\,\dot{\delta x} + \delta x\,\dot{\delta x} + y_0\,\dot{\delta y} + \delta y\,\dot{\delta y} \right) \\ \dot{I}_{xy} &= m_s\left(x_0\,\dot{\delta y} + y_0\,\dot{\delta x} + \dot{\delta x}\,\delta y + \dot{\delta y}\,\delta x \right) \\ \dot{I}_{xz} &= m_s\left(x_0\,\dot{\delta z} + z_0\,\dot{\delta x} + \dot{\delta x}\,\delta z + \dot{\delta z}\,\delta x \right) \\ \dot{I}_{yz} &= m_s\left(y_0\,\dot{\delta z} + z_0\,\dot{\delta y} + \dot{\delta y}\,\delta z + \dot{\delta z}\,\delta y \right) \end{aligned} \tag{5.2.7}$$

Observe that since the VSMW is restricted to changes along the *y* body axis,

$\delta x = \delta z = \dot{\delta x} = \dot{\delta z} = 0$ so that one can write:

$$\begin{aligned} \dot{I}_x &= 2m_s\left(y_0\,\dot{\delta y} + \delta y\,\dot{\delta y} \right) \\ \dot{I}_y &= 0 \\ \dot{I}_z &= 2m_s\left(y_0\,\dot{\delta y} + \delta y\,\dot{\delta y} \right) \\ \dot{I}_{xy} &= m_s\left(x_0\,\dot{\delta y} \right) \\ \dot{I}_{xz} &= 0 \\ \dot{I}_x &= m_s\left(z_0\,\dot{\delta y} \right) \end{aligned} \tag{5.2.8}$$

Substituting (5.2.8) into (5.2.3) yields:

$$\begin{aligned}
\Delta L &= 2m_s\left(y_0\,\dot{\delta}y+\dot{\delta}y\,\delta y\right)p-\dot{q}\,I_{xy}-m_s\left(x_0\,\dot{\delta}y\right)q-q^2I_{yz}+rpI_{xy}+r^2I_{yz}\\
\Delta M &= -\dot{p}\,I_{xy}-m_s\left(x_0\,\dot{\delta}y\right)p-\dot{r}\,I_{yz}-m_s\left(z_0\,\dot{\delta}y\right)r-rqI_{xy}+pqI_{yz}\\
\Delta N &= -\dot{q}\,I_{yz}-m_s\left(z_0\,\dot{\delta}y\right)q+2m_s\left(y_0\,\dot{\delta}y+\dot{\delta}y\,\delta y\right)r-p^2I_{xy}-rpI_{xz}+q^2I_{xy}
\end{aligned} \tag{5.2.9}$$

As expected, equations (5.2.9) show that the perturbation moment terms are functions of the moving section's mass, the displacement of its *cg* from the A/C *cg*, and the rate of extension of the moving portion. It is also a function of the angular velocities, *p, q, r* and inertial products, I_{xy} and I_{yz}.

Recall from equations (5.2.4) that:

$$\begin{aligned}
I_{xy} &= I_{xy_0}+m_s x(t)y(t)\\
I_{xz} &= I_{xz_0}+m_s x(t)z(t)\\
I_{yz} &= I_{yz_0}+m_s y(t)z(t)
\end{aligned}$$

When the aircraft is in a symmetric state, the *xz* plane is one of symmetry. Hence, by proper positioning of the body axis (in symmetric configuration) one can set $I_{xy_0}=I_{yz_0}=0$. For practical purposes, $I_{xz_0}\approx 0$

Therefore:

$$\begin{aligned}
I_{xy} &= m_s x_0 y\\
I_{xz} &= m_s x_0 z_0\\
I_{yz} &= m_s z_0 y
\end{aligned} \tag{5.2.10}$$

The mass, m_s of the moving section of the half wing assumes its maximum value as the half wing moves from a fully retracted state to a fully extended state in which case:

$$m_s = 2(mass_{element1} + mass_{element2}) + mass_{skin1} + mass_{skin2}$$

$$m_s \approx 5\text{lb mass} = 0.15\ slug$$

Figure 33 shows the cross-section of the spar and its elements. Note that at speeds of 80mph, and $\alpha = 8^{\circ}$, the VSMW can support loads of up to 3 slugs.

Hence, as an upper bound estimate, the mass of the moving section represents about 5% of the aircraft's total weight. See table 5 for aircraft dimensions.

Table 5: Aircraft Dimensions

Total A/C Mass	3 slugs
Mean Wing Thickness	0.17 ft
Mass of Moving Section	0.15 slug
Mass Half Wing	0.3 slug
Maximum full span	7.3 ft
Minimum full span	3.7 ft
Chord	1.2 ft

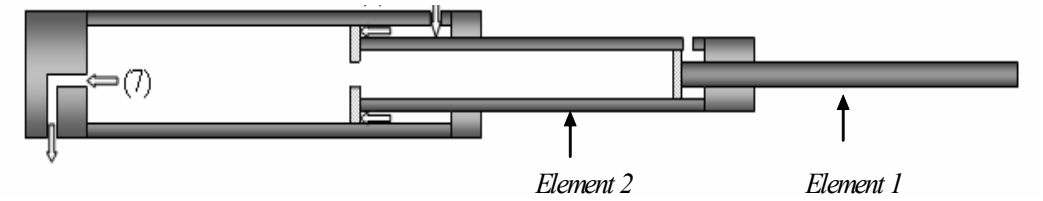

Figure 33: Location of Element 1 and Element 2

Assume that the *cg* of the moving element and the aircraft *cg* both lie in the *xz* plane, along the *y*-axis so that:

$$x_0 = z_0 = 0 \qquad (5.2.11)$$

For this case, it is therefore true that:

$$I_{xy} = m_s x_0 y = 0$$
$$I_{xz} = m_s x_0 z_0 = 0$$
$$I_{yz} = m_s z_0 y = 0$$

We are now justified in assuming that the inertial products are negligible. Hence, equations (5.2.9) reduce to:

$$\begin{aligned} \Delta L &= 2m_s \left(y_0 \dot{\delta y} + \dot{\delta y}\, \delta y \right) p = 2m_s \dot{\delta y} \left(y_0 p + \delta y p \right) \\ \Delta M &= 0 \\ \Delta N &= 2m_s \left(y_0 \dot{\delta y} + \dot{\delta y}\, \delta y \right) r = 2m_s \dot{\delta y} \left(y_0 r + \delta y r \right) \end{aligned} \tag{5.2.12}$$

Considering the sum of moments:

$$\begin{aligned} \sum L &= \sum L_0 + \Delta L = \dot{p} I_{x_0} + qr\left(I_{z_0} - I_{y_0} \right) + 2m_s \dot{\delta y} \left(y_0 p + \delta y p \right) \\ \sum M &= \sum M_0 + \Delta M = \dot{q} I_{y_0} + rq\left(I_{x_0} - I_{z_0} \right) \\ \sum N &= \sum N_0 + \Delta N = \dot{r} I_{z_0} + pq\left(I_{y_0} - I_{x_0} \right) + 2m_s \dot{\delta y} \left(y_0 r + \delta y r \right) \end{aligned} \tag{5.2.13}$$

We see that in the absence of inertial products, and geometry variations in *x* and *z* directions, the aircraft dynamics is strongly influenced by the span rate, $\dot{\delta y}$. Notice that if we set $\dot{\delta y}$=0 then:

$$\Delta L = \Delta M = \Delta N = 0 \tag{5.2.14}$$

Table 6 contains a summary of the dynamics equations. In it, we state the well-known aircraft force, and kinematic equations along with the full set of morphing moment equations derived in this section. Note that the force and kinematic equations are assumed to be identical for a morphing and conventional vehicle.

Table 6: Morphing Geometry Nonlinear Dynamics Equations

Exact Equations	$X - mg\sin\theta = M_t\left(\dot{u} + qw - rv\right)$ $Y + mg\cos\theta\sin\phi = M_t\left(\dot{v} + ru - pw\right)$ $Z + mg\cos\theta\cos\phi = M_t\left(\dot{w} + pv - qu\right)$ $\dot{\phi} = p + \tan\theta(q\sin\phi + r\cos\phi)$ $\dot{\theta} = q\cos\phi - r\sin\phi$ $\dot{\psi} = \frac{q\sin\phi + r\cos\phi}{\cos\theta}$ $p = \dot{\phi} - \dot{\psi}\sin\theta$ $q = \dot{\theta}\cos\phi + \dot{\psi}\cos\theta\sin\phi$ $r = \dot{\psi}\cos\theta\cos\phi - \dot{\theta}\sin\phi$ $\sum L = \sum\left(L_0 + \Delta L\right) = \dot{p}I_x + p\dot{I}_x - \dot{q}I_{xy} - q\dot{I}_{xy} - \dot{r}I_{xz} - r\dot{I}_{xz} \ldots$ $-qpI_{xz} - q^2I_{yz} + qrI_z + rpI_{xy} - rqI_y + r^2I_{yz}$ $\sum M = \sum\left(M_0 + \Delta M\right) = \dot{q}I_y + q\dot{I}_y - \dot{p}I_{xy} - p\dot{I}_{xy} - \dot{r}I_{yz} - r\dot{I}_{yz} \ldots$ $+rqI_x - rqI_{xy} - r^2I_{xz} + p^2I_{xz} + pqI_{yz} - rqI_z$ $\sum N = \sum\left(N_0 + \Delta N\right) = \dot{r}I_z + r\dot{I}_z - \dot{p}I_{xz} - p\dot{I}_{xz} - \dot{q}I_{yz} - q\dot{I}_{yz} \ldots$ $-p^2I_{xy} + pqI_y - prI_{yz} - qpI_x + q^2I_{xy} + qrI_{xz}$
Assume: $I_{xy}=I_{yz}=I_{xz}=0$	Force and Kinematic Equations assumed same as above. $\sum L = \dot{p}I_{x_0} + qr\left(I_{z_0} - I_{y_0}\right) + 2m_s\,\delta\dot{y}\left(y_0p + \delta yp\right)$ $\sum M = \dot{q}I_{y_0} + rq\left(I_{x_0} - I_{z_0}\right)$ $\sum N = \dot{r}I_{z_0} + pq\left(I_{y_0} - I_{x_0}\right) + 2m_s\,\delta\dot{y}\left(y_0r + \delta yr\right)$

5.3 Special Case of a Steady Roll

In this section we demonstrate that for a steady roll, equations (5.2.12) reduce to very simple expressions. To this end we use the kinematics equations given in [28]:

$$\begin{aligned} \dot{\phi} &= p + \tan\theta(q\sin\phi + r\cos\phi) \\ \dot{\theta} &= q\cos\phi - r\sin\phi \\ \dot{\psi} &= \frac{q\sin\phi + r\cos\phi}{\cos\theta} \end{aligned} \tag{5.3.1}$$

$$\begin{aligned} p &= \dot{\phi} - \dot{\psi}\sin\theta \\ q &= \dot{\theta}\cos\phi + \dot{\psi}\cos\theta\sin\phi \\ r &= \dot{\psi}\cos\theta\cos\phi - \dot{\theta}\sin\phi \end{aligned} \tag{5.3.2}$$

The kinematics equations describe the relationship between the Euler rates, $\dot{\phi},\dot{\theta},\dot{\psi}$, the Euler angles ϕ,θ,ψ and the body angular rates, *p, q, r.* In this analysis we only consider steady flight conditions that involve changes in the roll angle. Accordingly, we only consider the steady roll where $\dot{\phi}$ is constant and the following conditions hold [29]:

$$\dot{\theta},\dot{\psi} \equiv 0 \tag{5.3.3}$$

Substituting (5.3.3) into (5.3.2) yields:

$$\begin{aligned} p &= \dot{\phi} \\ q &= 0 \\ r &= 0 \end{aligned} \tag{5.3.4}$$

Substituting into equations (5.2.12):

$$\Delta L = 2m_s\,\dot{\delta y}\left(y_0 p + \delta y p\right)$$
$$\Delta M = 0$$
$$\Delta N = 2m_s\,\dot{\delta y}\left(y_0 r + \delta y r\right)$$

yields:

$$\begin{aligned} \Delta L &= 2m_s\,\dot{\delta y}\left(y_0 p + \delta y p\right) \\ \Delta M &= 0 \\ \Delta N &= 0 \end{aligned} \tag{5.3.5}$$

Therefore:

$$\begin{aligned} \sum L &= \dot{p}\, I_{x_0} + 2m_s\,\dot{\delta y}\left(y_0 p + \delta y p\right) \\ \sum M &= 0 \\ \sum N &= 0 \end{aligned} \tag{5.3.6}$$

A dimensional check reveals that the perturbation term in equation (5.3.6) does indeed have the units of moment.

Table 7: Special Case of a Steady Roll

Assumptions: Inertial products are negligible Steady Roll $\dot{\psi} = \dot{\theta} = 0 \Rightarrow q = r = 0$ $p = \dot{\phi}$	$X - mg\sin\theta = M_t\left(\dot{u} + qw - rv\right)$ $Y + mg\cos\theta\sin\phi = M_t\left(\dot{v} + ru - pw\right)$ $Z + mg\cos\theta\cos\phi = M_t\left(\dot{w} + pv - qu\right)$ $\dot{\phi} = p$ $\dot{\theta} = 0$ $\dot{\psi} = 0$ $p = \dot{\phi}$ $q = 0$ $r = 0$ $\sum L = \dot{p} I_{x_0} + 2m_s \dot{\delta y}\left(y_0 p + \delta y p\right)$ $\sum M = 0$ $\sum N = 0$
Assume *A/C cg* and moving section cg lie in *xz* plane along *y* axis	$\sum L = \dot{p} I_{x_0} + 2m_s \dot{\delta y}\left(y_0 p + \delta y p\right)$ $\sum M = 0$ $\sum N = 0$

5.4 Aerodynamic Considerations

5.4.1 Ordinary Differential Equation (ODE) Describing Steady Roll by VSWM

Having derived the full, nonlinear, inertia-based dynamic equations and simplifying to the case of a pure roll, it is important that we incorporate aerodynamic effects into the roll moment equation and compare it with that of a conventional aircraft that uses ailerons for roll control. In this section we develop the single degree of freedom model for an aircraft using span extension for roll control and compare it with the well-known single degree of freedom model for a conventional aircraft. It becomes clear that ΔL assumes the behavior of a damping term.

Consider the well-known equation of motion for a conventional aircraft executing a pure roll by means of ailerons:

$$\sum L = I_x \ddot{\phi} \tag{5.4.1}$$

$$\sum L = \frac{\partial L}{\partial \delta_{ail}} \delta_{ail} + \frac{\partial L}{\partial p} p \tag{5.4.2}$$

where $\frac{\partial L}{\partial \delta_{ail}} \delta_{ail}$ is the roll moment due to aileron deflection and $\frac{\partial L}{\partial p} p$ is the damping roll moment due to roll rate. Likewise, for span morphing, one can write:

$$\sum L = \frac{\partial L}{\partial \delta y} \delta y + \frac{\partial L}{\partial p} p \tag{5.4.3}$$

The first term on the right hand side is the roll moment due to span differential δy.

But, from equations (5.3.6):

$$\sum L = \dot{p} I_{x_0} + 2m_s \dot{\delta y}\left(y_0 p + \delta y p\right)$$

Therefore:

$$\frac{\partial L}{\partial \delta y}\delta y + \frac{\partial L}{\partial p} p - 2m_s \dot{\delta y}\left(y_0 + \delta y\right) p = \dot{p} I_{x_0} \tag{5.4.4}$$

$$\frac{\partial L}{\partial \delta y}\delta y + \left(\frac{\partial L}{\partial p} - 2m_s \dot{\delta y}\left(y_0 + \delta y\right)\right) p = \dot{p} I_{x_0} \tag{5.4.5}$$

Note that for a given telescoping mechanism, $\dot{\delta y}$ is some known constant, and m_s is also known. The baseline, symmetric term y_0 is also a known quantity. Furthermore:

$$\delta y = \int_{t_0}^{t_1} \dot{\delta y}$$

where t_0 and t_1 are the times at the initiation and completion of the extension or retraction. Hence for a given aircraft, using a particular telescoping mechanism, the quantity $2m_s \dot{\delta y}\left(y_0 + \delta y\right)$ is a constant, n_0.

$$2m_s \dot{\delta y}\left(y_0 + \delta y\right) = n_0$$

Therefore:

$$\frac{\partial L}{\partial \delta y}\delta y + \left(\frac{\partial L}{\partial p} - n_0\right) p = \dot{p} I_{x_0} \tag{5.4.6}$$

This is the ordinary differential equation that describes the behavior of an aircraft that uses VSWM to execute a steady roll.

Observe that $\left(\frac{\partial L}{\partial p} - n_0\right)$ is the term that describes aerodynamic damping due to roll rate.

It is well known that $\frac{\partial L}{\partial p}$ is inherently negative. Moreover, n_0 can assume positive or negative values depending on whether the wing is extending ($\dot{\delta y} > 0$) or retracting ($\dot{\delta y} < 0$). It is helpful to write:

$$\left(\frac{\partial L}{\partial p} - n_0\right) = -\left(\left|\frac{\partial L}{\partial p}\right| + n_0\right) \tag{5.4.7}$$

It is clear that n_0 serves to modify the total damping in the system. When $\dot{\delta y} > 0$, n_0 increases the total damping, consequently slowing down the roll. Conversely, for $\dot{\delta y} < 0$, one sees that n_0 decreases the damping, consequently speeding up the roll motion. This type of behavior is not surprising. It is simply a consequence of the law of conservation of angular momentum. As the total span increases, the angular velocity decreases. Conversely a decrease in span results in an increase in angular velocity.

Note also the dependence of n_0 on the y_0 term. Recall that y_0 is the initial y-coordinate of the moving section *cg* relative to the A/C *cg*. The location of y_0 can change since the elements of the spar are free to move relative to each other. Hence, as y_0 varies, the initial location of the moving section moves away from, or toward the wing tip.

Consider some initial symmetric span, y_0 as the starting point for span extension. For positive span rates, as y_0 increases, the damping term n_0 increases, causing the

subsequent motion to damp out more rapidly. Conversely, for $\dot{\delta y} > 0$, as y_0 decreases there is a commensurate decrease in damping. For negative span rates the opposite is true. Increasing y_0 serves to decrease the damping, whereas decreasing y_0 increases the damping.

5.4.2 Comparison between VSMW ODE and Aileron ODE

Let us compare the differential equation that describes roll motion from VSWM with that describing roll motion from aileron deflection:

$$\sum L = \frac{\partial L}{\partial \delta y}\delta y + \left(\frac{\partial L}{\partial p} - n_0\right)p \tag{5.4.8}$$

$$\sum L = \frac{\partial L}{\partial \delta_{ail}}\delta_{ail} + \frac{\partial L}{\partial p}p \tag{5.4.9}$$

Table 8: Comparison between 1-DOF Aileron Model and 1-DOF Variable Span Model

Single DOF Aileron Model	$\sum L = \frac{\partial L}{\partial \delta_{ail}}\delta_{ail} + \frac{\partial L}{\partial p}p$
Single DOF VSMW Model	$\sum L = \frac{\partial L}{\partial \delta y}\delta y + \left(\frac{\partial L}{\partial p} - n_0\right)p$ $n_0 = 2m_s\dot{\delta y}\left(y_0 + \delta y\right)$

Define the following:

$$\tau = -\frac{1}{L_p}$$

$$\tau^* = -\frac{1}{L_p^*}$$

$$L_p = \frac{\partial L / \partial p}{I_x}$$

$$L_p^* = \frac{\partial L / \partial p - n_0}{I_{x_0}} \tag{5.4.10}$$

$$L_{\delta a} = \frac{\partial L / \partial \delta a}{I_x}$$

$$L_{\delta y} = \frac{\partial L / \partial \delta y}{I_{x_0}}$$

The well-known solution to equations (5.4.8) and (5.4.9) are as follows:

$$p(t) = -\frac{L_{\delta a}}{L_p}\left(1 - e^{\frac{t}{\tau}}\right)\delta a \tag{5.4.11}$$

$$p^*(t) = -\frac{L_{\delta y}}{L_p^*}\left(1 - e^{\frac{t}{\tau^*}}\right)\delta y \tag{5.4.12}$$

Furthermore, the steady state roll rate is known to be:

$$p_{ss} = \frac{-L_{\delta_{ail}}}{L_p}\delta_{ail} \tag{5.4.13}$$

$$p_{ss}^* = \frac{-L_{\delta y}}{L_p^*}\delta y \tag{5.4.14}$$

It is clear that the span *extension* induces a damping roll moment that is greater than that due to aileron deflection. In chapter 4, we determined that for the wing under consideration, $\frac{\partial L}{\partial \delta y}\delta y$ can assume a value equivalent to, or even larger than $\frac{\partial L}{\partial \delta_{ail}}\delta_{ail}$.

For the purposes of argument let us assume that:

$$\frac{\partial L}{\partial \delta y}\delta y = \frac{\partial L}{\partial \delta_{ail}}\delta_{ail} \tag{5.4.15}$$

A steady state condition is achieved when the sum of the rolling moments vanishes. If equation (5.4.15) holds, then, from the definition of time constant in equations (5.4.10) one sees that the aircraft using a span extension for roll control has a smaller time constant τ. As a result, it will achieve steady state faster than one using ailerons. Furthermore, from equation (5.4.13) we see that in this case, $p^*_{ss} < p_{ss}$.

Consider the case where $\frac{\partial L}{\partial \delta_{ail}}\delta_{ail} < \frac{\partial L}{\partial \delta y}\delta y$. Furthermore, assume $n_0 \approx 0$. In this case, it is clear that $p^*_{ss} > p_{ss}$. For most practical purposes, the damping term n_0 may be small. Hence, if one were to consider solely the effect of an increased driving moment, $\frac{\partial L}{\partial \delta y}\delta y$, it is clear that $p^*_{ss} > p_{ss}$ and $\tau^* = \tau$. Therefore, one can conjecture that if n_0 is small in comparison to $\frac{\partial L}{\partial p}$, and if $\frac{\partial L}{\partial \delta_{ail}}\delta_{ail} < \frac{\partial L}{\partial \delta y}\delta y$, the aircraft using VSWM for roll control achieves a larger steady state roll rate in approximately the same time as one using ailerons.

Chapter 6: Conclusions and Future Work

In this chapter, we summarize the work that has been done and the contributions that have been made to the state of the art. Additionally, we make recommendations for future work.

This thesis has presented variable span wing morphing (VSWM) as an effector of roll control for unmanned aerial vehicles (UAVs). The roll coefficients obtained from VSWM have been quantified by theoretical and experimental data and compared with typical aileron roll moments. We see that small changes in span are an effective alternative to conventional ailerons for roll control. The standard six-degree of freedom (6-DOF) model that describes aircraft dynamics has been revisited. Simple expressions have been derived for the additional terms due to morphing. In particular, the special case of a steady roll was considered. The resulting ordinary, first-order differential equation illustrates a critical difference between an aircraft using variable-span morphing for roll control and one that uses ailerons for roll control: variable span morphing modifies the total system damping

In this study we assumed that the aircraft *cg* location was fixed with the wing *cg* free to move. In reality, morphing causes the aircraft *cg* to migrate along the *y*-body axis. The moving center of gravity presents unique challenges to the use of a VSMW for roll control. It is known that, for the wing under consideration, the moment due to the weight is small in comparison with that from the lift. However, further work needs to be done to determine the effect on stability of a migrating center of gravity.

Observe that this work only considers the morphing of one half-wing. The other was held at a constant span. The effect of morphing both wings simultaneously also needs to be considered. That is, one needs to consider the effect of increasing one half span by some amount δy while decreasing the other half span by the same amount. A main advantage of this method is that the total lift remains constant since the total span is invariant.

In order to accurately quantify the relationship between VSMW and aileron roll coefficients one needs to develop a normalization method that would account for the differences between variable span and variable aileron deflection.

The interference effect described in chapter 4 needs to be investigated more fully. This is important because in regions close to the wing-fuselage interface the roll coefficients no longer exhibit the predicted linear trend. Furthermore, this effect serves to decrease the available roll coefficients.

Bibliography

[1] R. W Wlezein, G. C Horner, A. McGowan, S. I Padula, M.A Scott, R. J Silcox and J. O Simpson "The Aircraft Morphing Program" AIAA Paper, 1998-1927, AIAA/ASME/ASCE/AHS/ASC Structures, Structural Dynamics and Materials Conference and Exhibit 39th and AIAA ASME AHS Adaptive Structures Forum, Long Beach, CA, April 1998

[2] Bowman, J., Sanders, B., and Weisshaar, T., "Evaluating the Impact of Morphing Technologies on Aircraft Performance," AIAA Paper 2002-1631, April 2002

[3] Blondeau J. E., "Development and Testing of a Variable Aspect Ratio Wing Using Pneumatic Telescopic Spars", Master's thesis University of Maryland 2004

[4] McCormick, Barnes, *Aerodynamics, Aeronautics and Flight Mechanics,* 2nd ed., Wiley, New York, 1995, p. 514

[5] Parker, H.F, "The Parker Variable Camber Wing," Report #77 Fifth Annual Report, National Advisory Committee for Aeronautics, Washington D.C, 1920

[6] Shavrov, V. B, History of Aircraft Construction in the USSR, Russian Aeronautical Education Series Publishers, Moscow, Russia, 1968

[7] Anderson, John D., *Modern Compressible flow*, 3rd ed., McGraw Hill, New York, 2003, p.346

[8] Anderson, John D., *Introduction to Flight*, 3rd ed., McGraw Hill, New York, 1989, p.27

[9] Anderson, John D., *Fundamentals of Aerodynamics*, 2nd ed., McGraw Hill, New York, 1984, p.343

[10] www.worldhistory.com/wiki/B/B-1-Lancer.htm

[11] www.worldhistory.com/wiki/F/F-14-Tomcat.htm

[12] http://www.airracinghistory.freeola.com/aircraft/Dayton%20Wright%20racer.htm

[13] Poonsong, P., "Design and Analysis of a Multi-Section Variable Camber Wing" Master's thesis, The University of Maryland, 2004

[14] Murray, J. E., Pahle, J. W., Thornton, S. V., Vogus, Frackowiak, T., Mello J. D., and Norton, B., "Ground and Flight Evaluation of a Small-Scale Inflatable-Winged Aircraft", AIAA Paper No. 2002-0820, AIAA Aerospace Sciences Meeting & Exhibit, 40th, Reno, NV, Jan 14-17, 2002

[15] Gevers, David, E., Gevers Aircraft Inc. "Multi-Purpose Aircraft", United States Patents Office, Patent Number 5,645, 250, July 1997

[16] McFarland, Marvin W. (ed.), *The Papers of Wilbur and Orville Wright*, McGraw-Hill, New York 1953

[17] Gibbs-Smith, C. H., *Aviation: An Historical Survey from its Origins to the End of World War II*, Her Majesty's Stationery Office London, 1970

[18] AAA, Advanced Aircraft Analysis, Software Package, Version 2.5, Lawrence, KS

[19] Roskam, J., and Kohlman, D. L., "Spoilers for Roll Control of Light Airplanes", AIAA Paper No. 74-861, AIAA Mechanics and Control of Flight Conference, Anaheim, CA, August 5-9, 1974

[20] Smith, J., "Alternative Methods of Roll Control for the Wide-Area Surveillance Projectile", Final Report 16.622 MIT, 2001

[21] The Flyer Assembly, US Patent No. 6,392,213 B1, issued May 21, 2002

[22] Boothe, K., "Dynamic Modeling and Flight Control of Morphing Air Vehicles", Master's thesis University of Florida 2004

[23] Garcia H. M., "Control of Micro Air Vehicles using Wing Morphing", Master's Thesis University of Florida 2003

[24] Ljung, L., *System Identification: Theory for the User, Prentice Hall*, Englewood Cliffs, NJ 1987

[25] Davidson, John B., Chwalowski and Lazos, Barry S., "Flight Dynamic Simulation Assessment of a Morphable Hyper-Elliptic Cambered Span Winged Configuration", AIAA Paper 2003-5301, AIAA Atmospheric Flight Mechanics Conference and Exhibit, August 2003, Austin, TX

[26] Blondeau, J., and Pines D., "Pneumatic Morphing Aspect Ratio Wing" AIAA-2004-1808 45th AIAA/ASME/ASCE/AHS/ASC Structures, Structural Dynamics and Materials Conference, Palm Springs, California, Apr. 19-22, 2004

[27] Raymer, Daniel, P. Aircraft Design: A Conceptual Approach, 3rd ed., AIAA Education Series, Virginia, 1999, p.126

[28] Nelson, Robert C., *Flight Stability and Automatic Control* 1st ed., McGraw-Hill 1989, p.92

[29] Stevens, Brian L., and Lewis, Frank L., *Aircraft Control and Simulation*, 1st ed., Wiley Interscience1992, p.81